Geochemistry, Geophysics, Geosystems

RESEARCH ARTICLE
10.1029/2019GC008862

Subduction Duration and Slab Dip

Jiashun Hu[1] **and Michael Gurnis**[1]

[1]Seismological Laboratory, California Institute of Technology, Pasadena, CA, USA

Key Points:
- Slab dip depends on subduction duration, where older subduction systems tend to have shallower slabs
- Long-term subduction duration is more significant than the latest reinitiation age in controlling slab dips
- The nature of overriding plate, continental versus oceanic plate, slab age, and convergence rate could influence dip angles

Supporting Information:
- Supporting Information S1
- Table S1
- Table S2

Correspondence to:
J. Hu,
jiashun@caltech.edu

Citation:
Hu, J., & Gurnis, M. (2020). Subduction duration and slab dip. *Geochemistry, Geophysics, Geosystems*, *21*, e2019GC008862. https://doi.org/10.1029/2019GC008862

Received 10 DEC 2019
Accepted 5 MAR 2020
Accepted article online 9 MAR 2020

Abstract The dip angles of slabs are among the clearest characteristics of subduction zones, but the factors that control them remain obscure. Here, slab dip angles and subduction parameters, including subduction duration, the nature of the overriding plate, slab age, and convergence rate, are determined for 153 transects along subduction zones for the present day. We present a comprehensive tabulation of subduction duration based on isotopic ages of arc initiation and stratigraphic, structural, plate tectonic and seismic indicators of subduction initiation. We present two ages for subduction zones, a long-term age and a reinitiation age. Using cross correlation and multivariate regression, we find that (1) subduction duration is the primary parameter controlling slab dips with slabs tending to have shallower dips at subduction zones that have been in existence longer; (2) the long-term age of subduction duration better explains variation of shallow dip than reinitiation age; (3) overriding plate nature could influence shallow dip angle, where slabs below continents tend to have shallower dips; (4) slab age contributes to slab dip, with younger slabs having steeper shallow dips; and (5) the relations between slab dip and subduction parameters are depth dependent, where the ability of subduction duration and overriding plate nature to explain observed variation decreases with depth. The analysis emphasizes the importance of subduction history and the long-term regional state of a subduction zone in determining slab dip and is consistent with mechanical models of subduction.

1. Introduction

The geometry of slabs and subduction dynamics are intimately related. A fundamental attribute of slab geometry is their dip. The controls on slab dip have been a topic of considerable discussion through analysis of measured attributes and theoretical and computational study (e.g., Gurnis & Hager, 1988; Jarrard, 1986; Lallemand et al., 2005). There should be correlation with the forces and kinematics of subduction, but empirical correlations have been characterized by a high degree of variance between multiple parameters. Statistical analysis of the empirical relation between slab dips and slab age, convergence rate, overriding plate nature, subduction polarity, and related parameters have been carried out. Jarrard (1986) suggested that subduction duration is statistically significant for predicting intermediate slab dip (down to 100 km) by analyzing 39 profiles averaged over modern subduction zones, but subduction duration has subsequently been ignored. Lallemand et al. (2005) expanded the data set to 159 transects and concluded that overriding plate motion plays an important role on slab dip angles, especially for slabs that penetrate into lower mantle. They found that retreating and oceanic overriding plates are often associated with steep slab dips, while advancing and continental overriding plates are usually associated with shallow slab dips.

The correlations between other subduction parameters and slab dips are often found to be weak or nonexistent. For example, Tovish and Schubert (1978) proposed that slab dip angle is a direct function of the radius of the arc curvature, but this was generally not observed at modern subduction zones (Schellart et al., 2004). Cruciani et al. (2005) measured slab dips down to 250 km along 164 sections and found no direct relation between dip angles and slab ages. The variation of dip angles was better explained by the combination of slab ages and subducting plate rate, but the correlation was not satisfactory. Schellart (2007) reported no observational basis to support the effect of subduction polarity on slab dip angles, negating the hypothesis of west drifting lithosphere relative to the asthenosphere (Doglioni et al., 1999; Moore, 1973; Uyeda & Kanamori, 1979).

Most recent statistical analyses after Jarrard (1986) are based on present-day observations of subduction zones. Parameters reflecting the time dependence of subduction are largely overlooked in parameter correlations. While studies have found good correlation between present-day parameters, such as overriding plate motion (Lallemand et al., 2005), significant unexplained variation of dip angles exists. Such variations

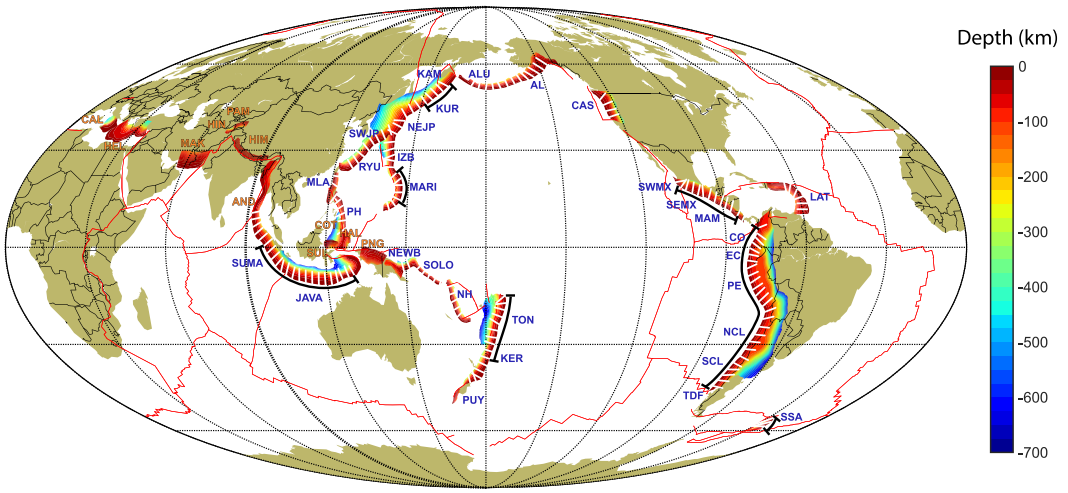

Figure 1. The location of the transects (white sticks) along subduction zones. Colored surface shows the depth of slab surface defined by *slab2* (Hayes et al., 2018). Thick black brackets highlight transects that penetrate into lower mantle, based on tomography models MITP2013 (Li et al., 2008), GAP_P4 (Obayashi et al., 2013), and LLNL_ G3Dv3 (Simmons et al., 2012). Subduction zones with blue names are used to generate the slab transects, while those with orange names are not used. PUY = Puysegur; KER = Kermadec; TON = Tonga; NH = New Hebrides; SOLO = Solomon; NEWB = New Britain; JAVA = Java; SUMA = Sumatra; AND = Andaman; COT = Cotabato; SUL = Sulawesi; HAL = Halmahera; PNG = New Guinea; MLA = Manila; PH = Philippine; RYU = Ryukyu; SWJP = SW Japan; MARI = Marianas; IZB = Izu-Bonin; NEJP = NE Japan; KUR = Kurile; KAM = Kamchatka; ALU = ALeutians; AL = Alaska; CAS = Cascades; SWMX = SW Mexico; SEMX = SE Mexico; MAM = Middle America; LAT = Lesser Antilles; CO = Columbia; EC = Ecuador; PE = Peru; NCL = North Chile; SCL = South Chile; TDF = Tierra del Fuego; SSA = South Sandwich; CAL = Calabria; HEL = Hellenic; MAK = Makran; HIN = Hindu Kush; PAM = Pamir; HIM = Himalaya.

can potentially be accounted for when taking an evolutionary perspective. This assertion needs to be placed within the context of numerical and laboratory experiments, which have shown that the average dip of slabs is strongly time dependent (e.g., Gurnis & Hager, 1988; Guillaume et al., 2009; Heuret et al., 2007). Although some models have indicated periods of slab flattening intervened by periods of slab steepening (e.g., Guillaume et al., 2009; Schellart, 2017) due to slab buckling, the long-term decrease of slab dip exists especially for subduction zones with trench retreat.

In this study, we measured slab dip angles of 153 transects (Figures 1 and S1) along subduction zones at present and compiled both the present-day observations of subduction parameters and evolutionary parameters based on the geological record and plate history, including subduction duration and total convergence. Readdressing the possibility that subduction duration is an important underlying control on slab dip is timely, given that the observational work on subduction initiation has progressed substantially since the appearance of these studies. With a larger data set and temporal parameters, we aim at developing an empirical relation between slab dip angles and subduction parameters that could better account for the variation of slab dips.

2. Slab Transects and Slab Dips

We use *slab2* (Hayes et al., 2018) to define slab dip angles (Figure 1). All the dip angles were extracted from the 153 transects that are normal to the trench along major subduction zones at present with an along-strike distance of 250 km (Figure 1). The geometry of the slab profile at these transects varies substantially (Figure S1). Different strategies have been used to define the shallow, deep, and/or intermediate dip angles in earlier studies. For example, Jarrard (1986) defined the shallow dip to be the dip from the trench to 60 km depth, the intermediate dip from the trench to 100 km depth, and the deep dip from 100 to 400 km; while Lallemand et al. (2005) defined the shallow dip to be the dip from trench to 125 km and the deep dip from 125 km to the maximum depth of the slab. In an analysis testing different strategies, we found the statistical behavior of the slab dips changes. Consequently, we define multiple dip angles, among which the shallow dip (α_s) is defined to be the dip from the trench to 100 km and five deep dips (from α_{d1} to α_{d5}) are subsequently defined

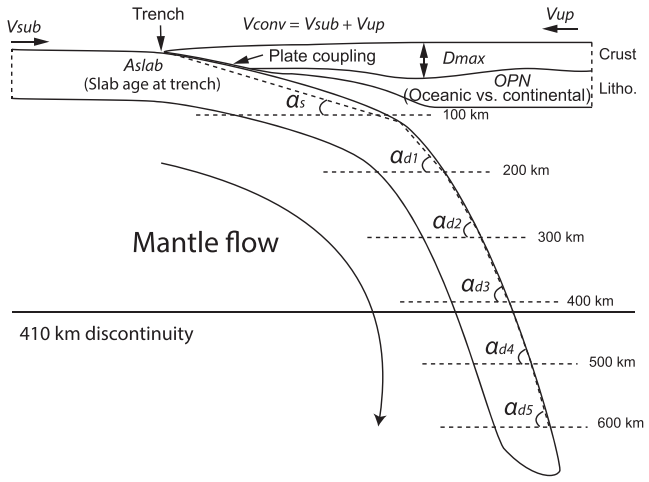

Figure 2. Schematic representation of slab dips and subduction parameters. The subducting plate rate V_{sub}, convergence rate V_{conv}, and the rate of upper plate motion V_{up} are all positive toward the trench. Only the trench-normal components of these parameters are used in the study. The maximum Moho depth D_{max} is measured within 300 km from the trench. α_s is shallow dip; α_d is deep dip; *OPN* is overriding plate nature; and A_{slab} is slab age at trench.

every 100 km until reaching 600 km depth (Figure 2). A total of six dips captures the major variation of dip angles along the slab profile and allows us to explore the depth-dependent statistical behavior of slab dips.

Compared to earlier studies (Jarrard, 1986; Lallemand et al., 2005), we used a more recent slab surface model, *slab2* (Hayes et al., 2018), for the extraction of slab dips. *slab2* has incorporated a comprehensive data set, including bathymetry, earthquake hypocenters, relocated hypocenters, active-source seismic reflection profiles, receiver functions, tomographic images, and other data types, and have provided a global high-resolution slab surface model (Figure 1). Compared to earlier studies that were based on earthquake hypocenters, *slab2* has a larger coverage, both horizontally and in depth. For example, *slab2* used receiver functions to extend the slab surface in Mexico from 70 km to more than 200 km in depth, which is mostly aseismic; this makes it possible to measure deep dip angles for the Middle American slab. The use of active-source and seismic reflection profiles helps in mapping the surface of the slab hinge, to which the shallow dips are quite sensitive. Finally, seismic tomography and receiver functions both help in correcting the slab surface at greater depths upward above earthquakes, improving the accuracy in determining slab deep dip angles.

In order to get a clearer empirical relation, we excluded a few subduction and collision zones that are either atypical or too complex to reliably determine the subduction zone parameters. For example, the subduction systems in Southeast Asia are complex. Current subduction is incipient, waning, or unknown (Jarrard, 1986), with the subduction parameters difficult to determine. We therefore have excluded the Cotabato, Halmahera, Sulawesi, and New Guinea subduction zones. Along the margin of Tibet, the Himalaya, Hindu Kush, and Pamir subduction zones are excluded, because they are continental collision zones. The Mediterranean has so much continental crust influencing the tectonics that the underlying geodynamic controls are unlikely to be simple expressed, so we have also excluded the Hellenic and Calabria subduction zones. The Makran subduction zone is excluded, because it is likely influenced by the continent-continent collision in the flanking Zagros and Hindu Kush regions and the fracture zone between Arabian and Indian Plate. Most of the Andaman Trench is characterized by purely strike-slip motion without much convergence going on. We therefore only keep the southernmost three transects where the motion of the two plates has a convergent component.

3. Data Set

3.1. Slab Age and Kinematic Parameters

We have estimated the present ages at the trenches as a proxy of slab ages (Figure 2), from the digital seafloor age grid (Müller et al., 1997) and online updates. Slab age varies with time as evident in plate reconstructions (e.g., Müller et al., 2008; Seton et al., 2012), but it is not straightforward to determine which age is most significant for slab dips, the present age, past age, or mean of the ages during a certain period. We simply used the present ages at the trenches to characterize slab ages. In addition, since the relation between slab dip and slab age is likely not linear, we also consider the square root of slab age, proportional to slab thickness, as an alternative parameter (Turcotte & Schubert, 1982).

The trench-normal components of the instantaneous kinematic parameters, including subducting plate rate, convergence rate, and overriding plate motion (Figure 2), are taken from a recent plate reconstruction by Seton et al. (2012). With this digital plate model and *pyGPlates*, we have also extracted the time-dependent kinematic parameter, total convergence, which is slab length subducted since the initiation of subduction.

3.2. Subduction Duration

How long a subduction zone has existed plays an important role governing the present geometry of subduction zone. Earlier, Jarrard (1986) noted a significant correlation between intermediate slab dip and the duration of subduction, subduction zones with shorter durations having steeper slab dips. Although diagnostic of geodynamic processes, this important parameter has been ignored in the decades because of perceived

Table 1
Initiation Ages for Active Subduction Zones

Symbol	Subduction zone	Method (reinitiation)	Latest initiation (reinitiation) (Ma)	Method (long-term)	Long-term age (Ma)	Arc age (Jarrard, 1986) (Ma)	References
PUY	Puysegur	SL	16–8	—	—	n/a	Sutherland et al. (2006); Gurnis et al. (2019)
KER	Kermadec	FA, UP	35		—	30 ± 2	Meffre et al. (2012); Sutherland et al. (2020)
Ton	Tonga	FA, UP	50		—	24 ± 7	Meffre et al. (2012); Sutherland et al. (2020)
NH	New Hebrides	UP, BA	14	—	—	8 ± 3	Macfarlane et al. (1988); Pelletier et al. (1993)
SOLO	Solomon	AA	8	—	—	8 ± 3	Petterson et al. (1999)
NEWB	New Britain	UP	8		—	8 ± 3	Lindley (2006)
JAVA	Java	AA, UP	70–50	AA, UP	170	27 ± 3	Clements and Hall (2011)
SUMA	Sumatra	AA, UP	70–50	AA, UP	170	27 ± 3	McCourt et al. (1996); Zahirovic et al. (2016)
AND	Andaman	AA	97–93	AA	—	100 ± 40	McCourt et al. (1996); Pedersen et al. (2010)
COT	Cotabato	AA	12–5	—	—	n/a	Yumul et al. (2003)
MLA	Manila	AA	22–15	—	—	n/a	Yumul et al. (2003)
PH	Philippine	AA	5–3	—	—	6 ± 4	Yumul et al. (2003)
RYU	Ryukyu	SL	35–16	AC	201–145	55 ± 5	Ma et al. (2019); Miyazaki et al. (2016)
SWJP	SW Japan	AA	17	AC	201–145	175 ± 5	Kimura et al. (2005); Taira et al. (2016)
MARI	Marianas	FA	52–48		—	45 ± 5	Arculus et al. (2019)
IZB	Izu-Bonin	FA	52–48		—	45 ± 5	Arculus et al. (2019)
NEJP	NE Japan	AA, SL	60–46	AC	201–145	115 ± 5	Seton et al. (2015); Taira et al. (2016)
KUR	Kurile	AA, SL	60–46	—	—	82 ± 16	Seton et al. (2015)
KAM	Kamchatka	AA, SL	60–28	AA, AC	150	153 ± 10	Seton et al. (2015); Watson and Fujita (1985); Taira et al. (2016)
ALU	Aleutians	AA	69	—	—	56 ± 6	Hoernle et al. (2018)
AL	Alaska, Alaska Peninsula	AA	153–120	AA	230	160 ± 10	Amato and Pavlis (2010); Plafker et al. (1989)
CAS	Cascades	AA	53–48	AA	255	175 ± 10	Wells et al. (2014); Saleeby (2011)
SWMX	SW Mexico	—	—	AA, SL	220	90 ± 3	Boschman et al. (2018)
SEMX	SE Mexico	—	—	AA, SL	220	90 ± 3	Boschman et al. (2018)
MAM	Middle America	UP, AA	75–73	—	—	100 ± 10	Buchs et al. (2010)
LAT	Lesser Antilles	AA	59–38	AA	88	48 ± 4	Neill et al. (2011); Briden et al. (1979)

Table 1 *(continued)*

Symbol	Subduction zone	Method (reinitiation)	Latest initiation (reinitiation) (Ma)	Method (long-term)	Long-term age (Ma)	Arc age (Jarrard, 1986) (Ma)	References
CO	Columbia	—	—	AA	235–202	242 ± 5	Mpodozis and Ramos (1989)
EC	Ecuador	—	—	AA	235–202	226 ± 19	Mpodozis and Ramos (1989)
PE	Peru	—	—	AA	235–202	226 ± 19	Mpodozis and Ramos (1989)
NCL	North Chile	SL	90–60	AA	235–202	226 ± 19	Chen et al. (2019); Mpodozis and Ramos (1989)
SCL	South Chile	SL	50–39	AA	235–202	226 ± 19	Chen et al. (2019); Mpodozis and Ramos (1989)
TDF	Tierra del Fuego	SL	30–10	AA	176–161	164 ± 6	Chen et al. (2019); Mukasa and Dalziel (1996)
SSA	South Sandwich	BA	45	—	—	30	Barker (2001)

Abbreviations: AA = arc age; FA = forearc age; UP = uplift; SL = seismic length; BA = back-arc age; AC = accretionary complex.

difficulties and uncertainties constraining the duration of subduction. Given the past demonstration that it is a key control on the geodynamics of subduction combined with a resurgence of observational work on subduction initiation (Arculus et al., 2019; Gurnis et al., 2019; Hall, 2018), returning duration of subduction to the multivariate analysis of subduction parameters is warranted.

Although constraints on the true age of subduction initiation are growing, there are still limitations. Nevertheless, in a number of cases, we have found that the oldest related volcanics are similar to the ages proposed by Jarrard (1986), who in turn argued that his ages were not substantially different from those of Dickinson (1973). We describe the major updates made to subduction zone ages from the Jarrard (1986) compilation based on more recent work. For most subduction zones, Jarrard (1986) summarized what he termed arc age. Assuming that arc volcanism rapidly follows the initiation of subduction, the oldest known rocks provide a lower bound on the duration of subduction. The difference between the duration of subduction and arc age could be as long as about 15 Myr or as short as a few Myr, as shown by well-constrained Cenozoic subduction initiation events. For example, for the actively initiating Puysegur subduction zone, the duration between the onset of compression and volcanism may be 8–16 Myr (Sutherland et al., 2006), while for the well-known Izu-Bonin-Mariana system, it is likely to be only several million years based on comparing the volcanic stratigraphy of the inner trench wall with events that occurred just behind the nascent arc (Arculus et al., 2019). Arc age will be one of the means by which we will constrain subduction duration.

There are other means to estimate when subduction initiated. Important for some intraoceanic subduction zones is the oldest age of rocks sampled from the forearc that can be traced to subduction initiation. We will call these forearc ages. The start of back-arc spreading also places constraints on the duration of subduction as it must postdate initiation. For some long existing subduction zones, the age of an inferred accretionary complex, often with both sedimentary sections and intruded granitic bodies, has been used. In other cases, there have been structural changes that have led to uplift of the overriding plate that can be dated. Finally, seismic constraints, often associated with the length or continuity of the slab, have been combined to estimate the duration of subduction (seismic length). For some subduction zones, multiple constraints have been used to estimate the duration of subduction, and these secondary means have been noted in Table 1 as well. In the table, we have also noted the most pertinent references pertaining to our arguments on the duration of subduction.

An important component of uncertainty is the interpretation of hiatuses in the history of volcanic activity or changes in the character of volcanic activity, for example, associated with merging of a trench with a ridge. In some cases, bursts of volcanism have been interpreted in terms of continuing subduction despite the merging of a trench and ridge. The geodynamics between a subduction zone in which a new subduction zone

has just formed where there was none previously versus a hiatus in subduction caused either by subduction of a ridge or a change in convergence velocity are likely to be different. If other stratigraphic, structural, or seismic information suggests that subduction stopped and restarted later, we tabulate two different ages for the duration of subduction: one associated with the most recent reinitiation of subduction and the other with the longer-term arc age. Finally, when a subduction zone undergoes a polarity reversal, we assign an age to the newly formed system. Our discussion is organized by describing each zone in a clockwise circuit around the Pacific starting south of New Zealand and ending at the southern tip of South America.

We have included the Puysegur-Fiordland subduction zone in the southwest corner of the South Island of New Zealand. This subduction zone is so young, that plate convergence vectors over the Miocene together with the present-day shape and depth of the Benioff zone beneath Fiordland constrain the time the Australian Plate first underthrust the Pacific Plate to the range of 16–8 Ma (Sutherland et al., 2006). These ages are consistent with onshore rock uplift rates ascribed to subduction initiation (House et al., 2002, 2005) and with the age when oceanic plate first juxtaposed continental crust (Gurnis et al., 2019). Since subduction-related volcanism has only commenced within the last 1 Myr (with Ar-Ar ages varying between 350 and 20 Ka Mortimer et al., 2013), we assign the true age of subduction initiation, 16–8 Ma for our analysis.

We have given different ages for the initiation of Kermadec and Tonga subduction, as did Jarrard (1986). The oldest ages found on the Kermadec ridge center around 26 ± 2 Ma (Ballance et al., 1999). Earlier published ages were younger than this, although Jarrard assigned an age of 30 Ma. The oldest samples dated from ODP Site 841 hole on the Tonga forearc cluster around 45 Ma, with the oldest being a K-Ar age of 46 Ma (McDougall, 1994). More extensive dredging on the inner trench wall of the Tonga Trench reveals ages in the range of 51 to 49 Ma from U-Pb dates (Meffre et al., 2012). When the Tonga subduction zone initiated, it must have done so much further to the west of the present-day trench but no further than New Caledonia. U-Pb ages of zircons on New Caledonia of 44.1 ± 0.9 and 44.5 ± 1.2 Ma are consistent with eclogite metamorphism and obduction (Spandler et al., 2005). A 50 Ma initiation age for Tonga and 35 Ma for Kermadec are consistent with recently completed ocean drilling in the area of the Lord Howe Rise and Norfolk Ridge (Sutherland et al., 2020). The much more refined geochronological constraints allow us to assign an age of 50 Ma to Tonga, substantially older than the 24 Ma age of Jarrard (1986). Although Tonga-Kermadec is thought to have arisen at the position of an older arc (Sutherland et al., 2019), there is no compelling evidence for Late Cretaceous to Paleocene subduction regionally (Mortimer et al., 2018); thus, there is an approximately 60 million interval between the old subducting boundary and the new one.

Individually, the New Hebrides, Solomon, and New Britain subduction zone formed by polarity reversal from the former Vitiaz Trench and Melanesian arc in which the Pacific Plate had earlier subducted beneath the Australian; Jarrard assigns a uniform age of 8 ± 3 Ma to this reversal. Furthest to the east along the Melanesian arc is the New Hebrides island arc, which was active and emergent from 25 to about 14 Ma (Greene et al., 1994; Macfarlane et al., 1988). Volcanism ceased, and the chain became submergent between 14 and 11 Ma, presumably in response to cessation of southwest dipping subduction beneath the Vitiaz Trench (Macfarlane et al., 1988). At about 10 Ma, the western belt (closet to the present-day trench) became emergent and by 8 Ma volcanism initiated along the eastern belt. Macfarlane et al. (1988) suggest that the uplift of the western belt was the result of a compressive regime associated with initiation of eastward dipping subduction along the New Hebrides Trench. The maximum age of spreading in the North Fiji Basin is 14–12 Ma (Pelletier et al., 1993) consistent with an age of about 14 Ma for the start of subduction.

The Solomon Trench segment of the Melanesian arc shows a continuous evolution from the Eocene to the present. The history has been interpreted as a polarity reversal as the Ontong Java Plateau collided with the Vitiaz Trench. On Guadalcanal, the oldest age for the arc is a 6.4 ± 1.9 Ma K-Ar age (Petterson et al., 1999). According to Petterson et al. (1999), there is no definite evidence that arc volcanism began earlier than the latest Miocene (ca. 8 Ma), so the recent work confirms the age used by Jarrard (1986). For the New Britain segment, we assign the same age, 8 Ma, as formation of the New Britain and Cristobal Trenches formed by the same polarity reversal (Cooper & Taylor, 1985). This age is older than that of the associated Bismark Sea back-arc basin, which formed within the last 3.5 Myr (Taylor, 1979). New Britain presumably uplifted during subduction initiation as indicated by the generally flat lying late Miocene limestones, which occur over a substantial portion of the island (Lindley, 2006). Along the northern parts of the island, there are many Quaternary volcanics, arising from the new north-dipping subduction zone. The timing of the uplift of the limestone is poorly known (Lindley, 2006) but conceivably reflects the age of subduction initiation.

Although Hamilton (1979) described volcanic rocks through Sundaland back to 200 Ma and Jarrard (1986) assigned an age of 27 Ma for both Sumatra and Java, a more intermediate age of 60 Ma is preferred based on more recent data and interpretations of the plate tectonic history of Indonesia (Zahirovic et al., 2016). Continental fragments of East Java and West Sulawesi were approaching the Sundaland active margin in the Late Cretaceous, and a lack of volcanic-derived zircons after 80 Ma (Clements & Hall, 2011) suggested the end of subduction in Java as these terranes sutured to Sundaland. Further west at the Sumatra margin, subduction ceased by ~75 Ma consistent with a magmatic gap between ~75 and 60 Ma on Sumatra and a hiatus of subduction along this margin (McCourt et al., 1996). The resumption of subduction at 60 Ma is consistent with seismic images of the mantle and interpretations of the marine inundation of SE Asia (Zahirovic et al., 2016), where we assign a 70–50 Ma range based on the model resolution. The Andaman arc formed on oceanic crust and U-Pb zircon dating of rocks from South Andaman Island reveals an age of crustal formation of 95 ± 2 Ma (Pedersen et al., 2010), which we assigned to the initiation of this subduction zone. For the long-term age of subduction regionally, we use the ca. 170 Ma onset of arc volcanism in the Sumatra segment (McCourt et al., 1996).

The northern Philippine Islands are sandwiched between the opposite polarity Manila and Philippine Trenches, which date to the Cenozoic (Yumul et al., 2003). Yumul et al. (2003) argue that K-Ar dates of extrusive and intrusive rocks and paleontological dates of sedimentary formations constrain the initiation of the Manila Trench to ca. 22 Ma, with a 20–15 Ma range for the transition to the east-facing subduction system. We have chosen the structural arguments for the initiation of the Manila Trench instead of the ages of the volcanic rocks that make up the Luzon arc, as the earlier Cenozoic ages likely reflect earlier subduction along the East Luzon Trough (Yumul et al., 2008). The earliest rocks, ages >15 Ma, in the Luzon arc associated with the Manila Trench have adakitic compositions (Jego et al., 2005). Yumul et al. (2003) further argue that the Philippine Trench dates to the early Pliocene, 5–3 Ma, and the Cotabato Trench to the Late Miocene, 12–5 Ma. The Philippines also has evidence for other recent subduction initiation events for trenches that are no longer active, including a short-lived subduction zone within Palawan (Keenan et al., 2016).

Dating of the Izu-Bonin-Marianas subduction initiation primarily comes from direct sampling of the forearc with dredging and drilling. Dredging on the forearc in the southern Marianas reveals forearc basalts with a subduction signature having an Ar-Ar age of 51 Ma (Reagan et al., 2010) while 1,200 km to the north in the Bonin forearc comparable Ar-Ar ages of 52–49 Ma are found (Ishizuka et al., 2011). In both cases, the basalts are overlain by boninites with Ar-Ar ages of 48–44 Ma (Ishizuka et al., 2011). These ages are corroborated by the ages of the basement (mean of Ar-Ar ages being 48.1 Ma Ishizuka et al., 2018) upon which the new arc formed, but, if that basement formation leads to subduction initiation or was a consequence of initiation, remains unclear (Arculus et al., 2019; Leng & Gurnis, 2015). As the Bonin and the southern Mariana sections were only about 500 km apart, along strike, when they formed (Leng & Gurnis, 2015) and the ages for the volcanic stratigraphy are close and overlap, we have adopted a single age range of 52 to 48 Ma for the Izu-Bonin-Marianas subduction initiation event.

For the Ryukyu arc, as the Izu-Bonin arc rotated clockwise during the Cenozoic, there was a hiatus in the subduction of the Pacific Plate (broadly between 35 and 16 Ma) replaced by the subduction of the much younger West Philippine Sea Plate and consistent with a gap in the seismically imaged slab within the transition zone (Ma et al., 2019). Presumably, the change in the character of subduction leads to the rifting of the Okinawa Trough, a back-arc opening on the East Asia margin that commenced in the Miocene (Sibuet et al., 1987). For the earlier subduction history, we assign a broad 201 to 145 Ma age range along Ryukyu based on the distribution of accretionary deposits and volcanic rocks (Miyazaki et al., 2016).

With transform motion between the Pacific Plate and Japan, SW Japan underwent a period when subduction of the Pacific plate ceased but reinitiated at 17 Ma by subduction of younger Philippine Sea plate (Kimura et al., 2005). The main islands of Japan, both southwest and northeast Honshu, have been characterized as an accretionary complex with granitic volcanism indicative of subduction from at least the Jurassic (Taira et al., 2016). Since the history of accretion is long with a number of transcurrent displacements during the Jurassic (Taira et al., 2016), we have assigned a broad Jurassic age range to the long-term subduction duration, 201 to 145 Ma. On Kamchatka, there is little evidence for pre–Mesozoic rocks (Watson & Fujita, 1985). Based on volcanic rocks and evidence for convergence within Kamchatcha, we date the long-term duration of subduction to 150 Ma. But from Japan through to Kamchatka, the distribution of ages for subduction-related

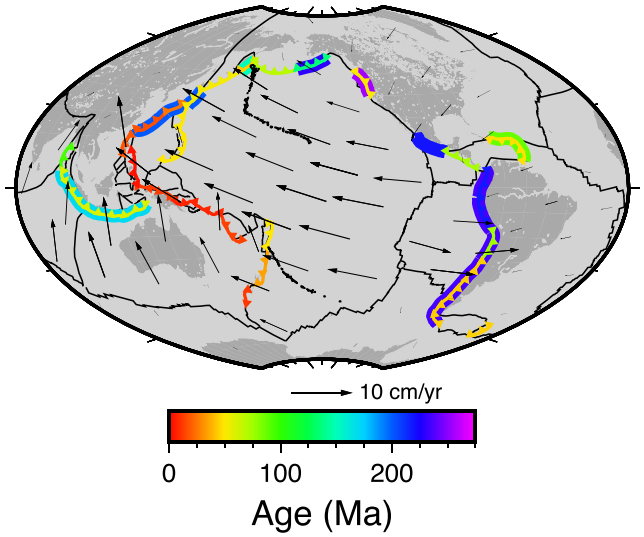

Figure 3. Distribution of subduction duration for major subduction zones. The colors of the trenches represent the latest initiation (reinitiation) age, while those of the underlying thick line represent the long-term age. Plate boundaries and absolute plate motions from Müller et al. (2016).

volcanism and interpretation of seismic tomography suggest a large-scale interruption of subduction associated with the merging of the Izanagi-Pacific spreading center with the trench from about 60 to potentially 46 Ma (Seton et al., 2015; Wu & Wu, 2019). We assign this age range to the reinitiation age for most of the region from Japan to Kamchatcha, except for SW Japan, which is even younger, as discussed above.

Although Ar-Ar ages for the Aleutians have suggested an onset of the arc from the middle Eocene (Jicha et al., 2006), and perhaps synchronous with the start of Izu-Bonin-Mariana and Tonga subduction, more complete sampling of Aleutian forearc canyons, reararc Kresta Ridge, Komandorsky Block, and Komandorsky Islands suggests an earlier onset of the arc. Using U-Pb zircon and Ar-Ar age-dating methods, Hoernle et al. (2018) show magmatism from 69 to 11 Ma. Consequently, we assign an age of 69 Ma for the Aleutians, although the eastern part of the arc may have started later (Hoernle et al., 2018). Prior to the onset of subduction initiation along the Aleutian arc, subduction occurred along the Beringian margin (current Alaska passive margin in the Bering Sea Scholl et al., 1986), which would have been linked with subduction along the Alaska subducting boundary. Alaska has been characterized as a subducting plate boundary since the late Paleozoic (Bond, 1973) and from the Late Triassic as a boundary with the accretion of a series of terrains and oceanic sediments (Plafker et al., 1989). One of those terrains was the north-dipping intraoceanic Talkeetna arc that amalgamated with the Wrangellia terrain (Rioux et al., 2007). If the volcanic evolution of the Talkeetna arc reflects conditions before accretion to North America (Rioux et al., 2007) or after (Plafker et al., 1989) remains to be determined. Given this uncertainty, we use the known range 153–120 Ma of U-Pb ages of detrital zircons within the Chugach terrain, south of the Talkeetna arc (Amato & Pavlis, 2010). We assign the Late Triassic age, 230 Ma (Plafker et al., 1989), to the longer-term age of subduction beneath Alaska and the Alaska Peninsula.

The Cascade, Mexican, and Middle American subduction zones are smaller remnants of the much longer subduction zone that existed on the western margin of North America. For the longer-term duration of the Cascades, we use the estimate for the initiation to be ~255 Ma of an ophiolite obduction in California based on U-Pb ages of both the protolith and metamorphism (Saleeby, 2011). This agrees with the initiation of arc magmatism along the eastern Sierra Nevada region (Saleeby, 2011). There have been interruptions in subduction along this margin, the latest associated with the obduction of the Siletzia terrain in the central part of the Cascadia subduction zone (Schmandt & Humphreys, 2011; Wells et al., 1984). Based on the combination of age dating of volcanic rocks, structural evolution and seismic evidence, the reinitiation of subduction has been dated at 50 Ma (Schmandt & Humphreys, 2011) with a 53–48 Ma range based on U-Pb ages of basalt eruptions (Wells et al., 2014). Through an interpretation of seismic tomography, along with paleomagnetism and other geological indicators, Boschman et al. (2018) assign a 220 Myr duration for subduction in Mexico. We assign this age to SW and SE Mexico, considerably longer than the 90 ±3 Ma age assigned by Jarrard (1986) and shorter than the 255 Ma geologically based age for North America. The subduction zone in Middle America, especially in southern Costa Rica and western Panama, has been dated at 75–73 Ma through combined tectonostratigraphic and petrologic study (Buchs et al., 2010). This is somewhat younger than the 100 Ma age assigned by Jarrard (1986). The new arc is thought to have formed at the boundary of an oceanic plateau between North and South America. The Caribbean region had been surrounded by different configurations of subduction since at least the Jurassic (Boschman et al., 2014). Ages for rocks recovered on the Aves Ridge, just to the west of the Antilles arc, suggest that the arc was active 88–59 Ma (Neill et al., 2011), and so we assign an age to the long-term duration of the Antilles at 88 Ma. Based on the K-Ar ages for the Antilles arc, which range in age back to 38 Ma (Briden et al., 1979), and sediment accumulation within the Barbados accretionary prism, Boschman et al. (2014) argue that the transition to the Lesser Antilles Arc took place between 59 and 38 Ma. We use this age range as the period for reinitiation of this arc.

There has been nearly continuous subduction along the western margin of South America since the Carboniferous, ca. 320 Ma (Domeier & Torsvik, 2014) following the accretion of the Chilenia terrane in the Late Devonian (Mpodozis & Ramos, 1989). The margin came to resemble the present Andes as early as the

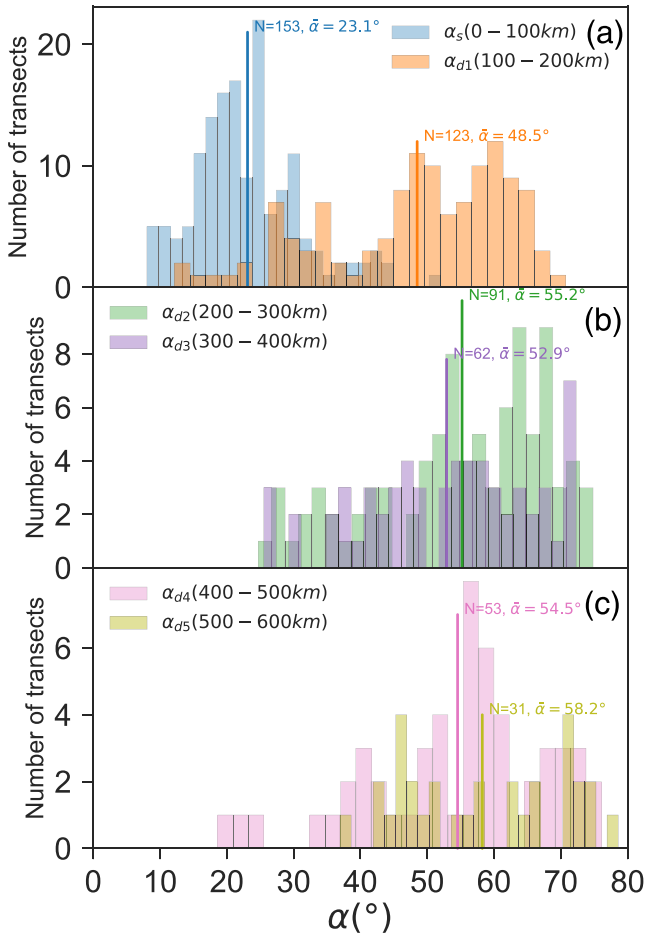

Figure 4. Distribution of slab dips among the 153 transects. (a) Dip angles that correspond to the two relatively shallow depth ranges of 0–100 km (α_s) and 100–200 km (α_{d1}); (b) dip angles that correspond to the two intermediate depth ranges of 200–300 km (α_{d2}) and 300–400 km (α_{d3}); and (c) dip angles that correspond to the two deep depth ranges of 400–500 km (α_{d4}) and 500–600 km (α_{d5}). The average dip angle within each group is marked by vertical lines, with total number of transects for each group indicated.

Triassic (Mpodozis & Ramos, 1989) about 235 to 202 Ma, not much different than the 226 Ma age adopted by Jarrard (1986). But after this period, there are hiatuses in volcanism and changes in arc chemistry and structural style that have mostly been interpreted in terms of changes in the dip angle of the subducting plate (slab flattening and slab steepening) and slab breakoff (Horton & Fuentes, 2016; Ramos & Folguera, 2009). Alternatively, Chen et al. (2019) argued that subduction along the entire Nazca Chilean margin terminated just before 80 Ma and then reinitiated from 80 to 40 Ma southward, with a 20 Myr range given for the ages. Although the gap in volcanism is short, and nonexistent at some latitudes, they argue that this is consistent with a gap in a seismically imaged slab in the lower mantle. The gap in the slab is not prominent in all tomography models, and Flament et al. (2014) have been able to match the seismically imaged slab from the upper mantle to core-mantle boundary with continuous subduction since the Jurassic in a plate tectonic-constrained mantle flow model. However, the change in structural style with time (from compression to extension during the early phases of subduction initiation) matches geodynamic predictions (Gurnis et al., 2004) on the evolution of the stress environment, and so we adopt the range of ages proposed by Chen et al. (2019) for the duration of subduction along this margin. Finally, at Tierra del Fuego, the ages of the granites there are as old as at least the Middle Jurassic, based on U-Pb ages (Mukasa & Dalziel, 1996), and so we update the 150 Ma age given by Jarrard (1986) for Tierra del Fuego. We assign 30 to 10 Ma reinitiation age for the southernmost Andes (Chen et al., 2019).

The South Sandwich forearc is currently unsampled, and so a reliable means to date the formation of this arc is not yet available. However, Barker (2001) has had the South Sandwich subduction zone starting at ~45 Ma through a polarity reversal from east dipping subduction beneath Chile and the Antarctic Peninsula to west dipping subduction below a proto–South Sandwich arc. We assign an age of 45 Ma to this subduction zone.

Due to the uncertainties, most of the compiled ages are shown as a range. We will simply use the middle age of the range for the analysis (Figure 3). In fact, using the minimum age or the maximum age of the range does not change the results (Figure S2). In some entries, either the latest initiation (reinitiation) age or the long-term age is missing, because these trenches have experienced continuous subduction since it was first initiated. For these cases, the same age will be used for both the latest initiation age and the long-term age.

3.3. Other Parameters

We have classified two groups of overriding plates (*OPN*) based on their crustal nature, either oceanic or continental. The maximum Moho depth within 300 km from the trench ($D_{\max}$) is determined using *Crust1.0* (Laske et al., 2013) to characterize the thickness of the overriding plate (Figure 2). Using recent tomography models including MITP2013 (Li et al., 2008), GAP_P4 (Obayashi et al., 2013), and LLNL_G3Dv3 (Simmons et al., 2012), we are able to determine the maximum depth of slab penetration that is categorized into one of three groups: apparently above 660 km (<660), apparently penetrate the transition zone (>660), and the rest (=660). All the parameters aforementioned are listed in Table S1.

3.4. Averaging Over Subduction Zones

When applying statistical analysis, Jarrard (1986) used subduction zone-averaged profiles, which means one profile for one subduction zone; alternatively, Lallemand et al. (2005) used multiple profiles for individual subduction zones. These densely sampled profiles in Lallemand et al. (2005) are able to capture the along-strike variation of slab dips and subduction parameters such as seafloor age, thus could help better resolve the empirical relations. In addition, including more data points helps improve the robustness of the

significance level of the predictors against outliers. Therefore, for most of the analysis, we will use multiple profiles for individual subduction zones.

On the other hand, this implies a larger weighting over longer subduction zones and a smaller weighting over shorter subduction zones. As an end-member case for the weighting strategy, we have also compiled the subduction zone-averaged data set by computing the mean dip angles and the mean subduction parameters over the subduction zones listed in Table 1. This produces 29 data points with each data point corresponding to one subduction zone (Table S2). We will perform statistical analysis for the shallow dips in this data set to verify the main conclusions. Since we have less data points for the deeper dips and the deep dips are difficult to explain even with the larger data set, the analysis with the smaller data set for the deep dips will be avoided.

4. Results

Measurement of slab dip angles gives a mean shallow dip of 23.1° ± 8.0° and mean deep dip of 48.5° ± 13.6° (α_{d1}), 55.2° ± 12.9° (α_{d2}), 52.9° ± 12.9° (α_{d3}), 54.5° ± 13.6° (α_{d4}), and 58.2° ± 12.1° (α_{d5}) (Figure 4). These values are similar to those of Jarrard (1986) where a mean "intermediate" dip (between 0 and 100 km) of 25.0° ± 8.8°and a mean deep dip (between 100 and 400 km) of 51.2° ± 19.1° were measured, although Jarrard (1986) only had 39 transects with each one representing the average of a whole subduction zone. Lallemand et al. (2005) sampled each subduction zone with multiple transects; their resultant mean shallow dip (between 0 and 125 km) of 32° ± 11° is slightly larger, while the mean deep dip (deeper than 125 km) of 58° ± 14° is largely similar to ours.

The six mean dip angles define an averaged slab profile, where the most gently dipping portion of the slab is controlled by the shallow dip angle (α_s), as indicated by the large difference (>25°) between the mean shallow dip and the mean deep dips. When looking at these dip angles individually (Figure 4), we find that the five deep dips have similar distributions, while the shallow dip angles consistently have smaller values, clearly distinguished from the deep dips. This further suggests that the shallow dip is the main controlling factor for slab shallowing.

4.1. Cross Correlations

We use the Pearson correlation coefficient (Pearson, 1895) to characterize the correlation between two variables (X, Y), $\rho_r = \mathrm{Cov}(X, Y)/(\sigma_X \sigma_Y)$, where Cov is the covariance and σ_X and σ_Y are the standard deviation of X and Y, respectively. The Pearson correlation has a value between −1 and +1, with +1 suggesting a perfect positive linear correlation, 0 no linear correlation, and −1 perfect negative linear correlation.

We first calculate the correlations between the shallow dip and the deep dips (Figure 5). The correlation coefficients are positive at shallow depth above 300 km and transition to negative values at greater depth below 400 km depth. This seems to suggest that the flatter the slab is at shallow depth (<300 km), the steeper it will be at greater depth. This trend is consistent with the configuration of a typical flat slab, which shows a sudden steepening following the flat portion such as in Peru and central Chile (Hayes et al., 2018; Hu & Liu, 2016).

The cross correlations between slab dip angles and subduction parameters are computed (Figure 6). We find that shallow dip correlates with subduction duration, with a Pearson correlation coefficient of −0.49 for the reinitiation age (A_{re}) and −0.70 for the long-term age (A_{long}) (Figures 6a and 6b). This suggests that older subduction systems tend to have shallower dips at shallow depth (<100 km), consistent with Jarrard (1986). Significantly, the long-term age clearly shows a stronger correlation with shallow dip than the reinitiation age. The shallow dip also correlates moderately with overriding plate nature, with a Pearson correlation coefficient of −0.51 (Figure 6e), suggesting that slabs subducting below continental plates tend to have smaller shallow dips. In contrast, the correlations between shallow dip angles and other subduction parameters, such as slab age, the square root of slab age, convergence rate, subducting plate rate, and overriding plate motion rate, are all weak or negligible (Figures 6c, 6d, and 6f–6h), consistent with the result of Cruciani et al. (2005) on slab age. This implies that these parameters are not the dominant controls over shallow dips. However, they may still contribute to the shallow dip variation, which we analyze with multivariate regression. The cross-correlation analysis for the subduction zone-averaged data set yields similar results (Figure S3), suggesting that the aforementioned patterns are robust regardless of the weighting strategy.

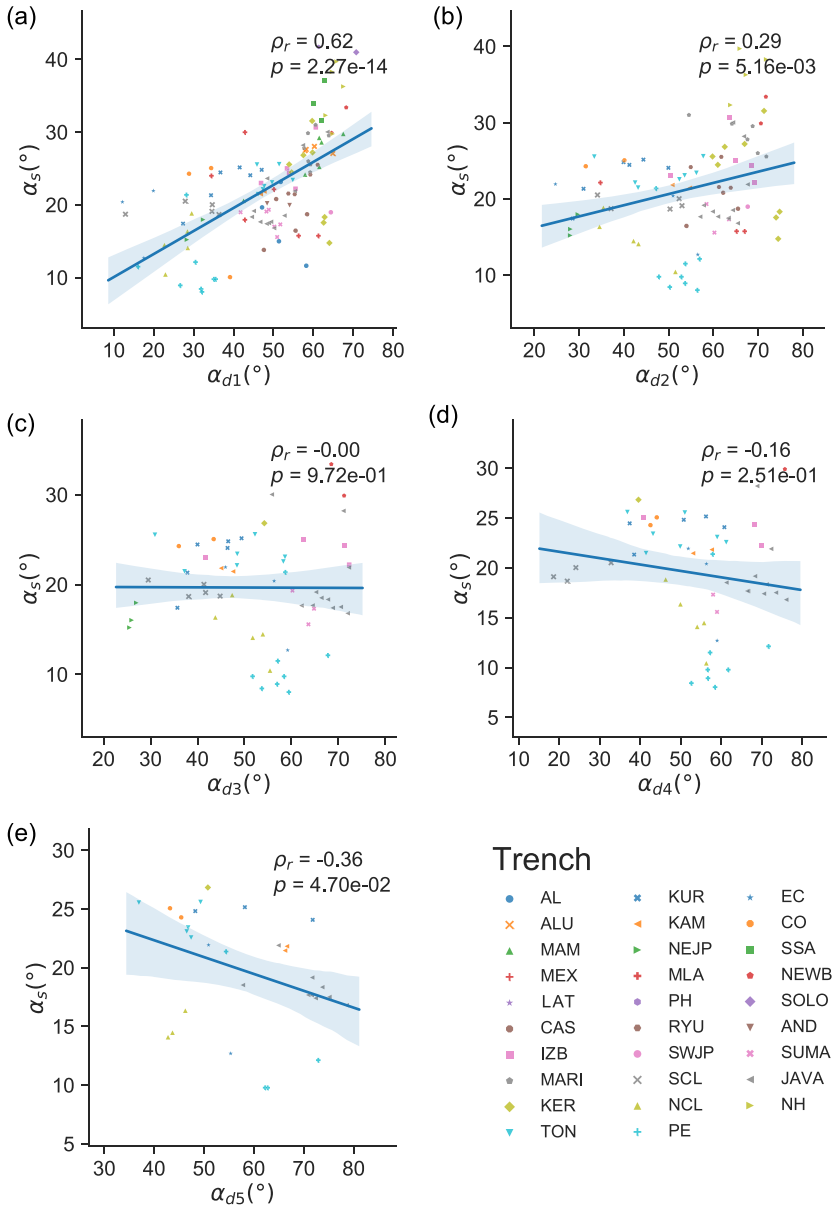

Figure 5. Correlation between the shallow dip and the deep dips:
(a) correlation between α_s and α_{d1}, (b) between α_s and α_{d2}, (c) between α_s and α_{d3}, (d) between α_s and α_{d4}, and (e) between α_s and α_{d5}. Different symbols represent transects along different trenches. Pearson correlation coefficient (ρ_r) and p value for the slope of the line are plotted for each panel. The blue shading represents the 95% confidence interval of the slope.

We also computed the correlation coefficients between the deep dips and the subduction parameters (Figure 7). Overall, the correlation between subduction duration and slab dip becomes weaker for dips measured at deeper depths. At depth below 300 km, the slab dips do not correlate with subduction duration. We observe a similar trend for overriding plate nature, except that the deepest dip (α_{d5}) and *OPN* become negatively correlated with a moderate Pearson correlation coefficient of −0.49. In contrast, we observe an overall stronger correlation between slab dips and slab age, overriding plate motion, subducting plate rate, and convergence rate, as the corresponding depths of slab dips increase (Figure 7). For example, these parameters are not correlated with the shallow dip (α_s), but they are moderately correlated with the deepest dip (α_{d5}). These patterns suggest that the behavior of slab dips is strongly depth dependent.

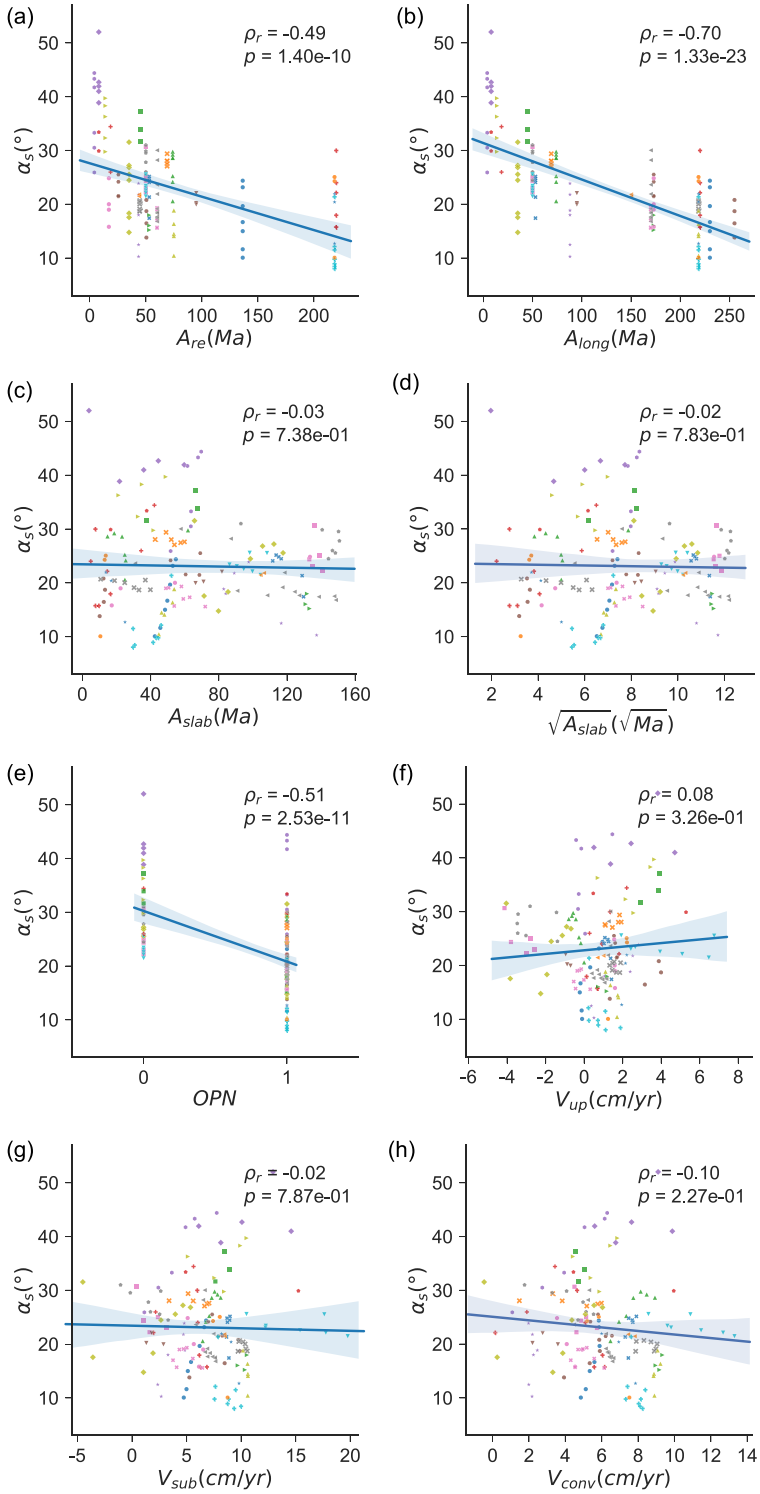

Figure 6. Correlation between shallow dip (α_s) and subduction parameters, including (a) subduction duration since the latest initiation (A_{re}), (b) subduction duration of the long-term age (A_{long}), (c) slab age (A_{slab}), (d) square root of the slab age ($\sqrt{A_{\text{slab}}}$), (e) overriding plate nature (*OPN*) with 1 on the horizontal axis representing continental plate and 0 representing oceanic plate, (f) the rate of upper plate motion (V_{up}), (g) subducting plate rate (V_{sub}), and (h) convergence rate (V_{conv}). Pearson correlation coefficient (ρ_r) and p value for the slope of the line are plotted for each panel. The blue shading represents the 95% confidence interval of the slope.

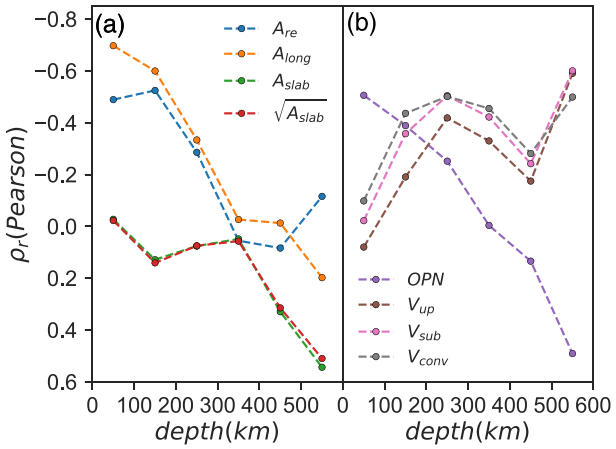

Figure 7. Depth-dependent correlation coefficients between slab dips and subduction parameters.

Lallemand et al. (2005) found a strong correlation between slab dip angles and the rate of overriding plate motion for slabs that extend below 660 km, while the correlation is weaker when all slabs are included. This implies that the dependence of slab dip angles may behave differently for slabs that have different length. To test this hypothesis, we compute the correlation coefficients between the shallow dip and subduction parameters for each group of slabs categorized by their maximum depths (Table 2). We find that the dependence of the shallow dip on subduction duration (both A_{long} and A_{re}) and overriding plate nature is generally consistent, with strong and moderate correlation for most of the groups. However, we do observe significant variation of correlation coefficients across different groups. For example, slab age has a weakly positive correlation with the shallow dip for slabs that are <660 km, while the correlation becomes moderately negative for slabs that are =660 km and becomes weakly positive again for slabs >660 km.

The kinematic parameters, including overriding plate motion, subducting plate rate, and convergence rate, show similar patterns as slab age (Table 2). However, the absolute correlation coefficients are generally smaller than or around 0.4, which indicates a weak correlation. Although the variation of these weak correlation coefficients may reflect some underlying mechanisms that are related to the maximum depth of a slab, they could be easily obscured by the large uncertainties due to the limited number of transects in the <660 and =660 km groups and the influence from other more dominant parameters. We emphasize that subduction duration, especially the long-term age, is the main controlling factor of the shallow dip for all the three categories.

Table 2
Correlations Between the Shallow Dip and Subduction Parameters for Different Groups of Slabs

A_{re}	A_{long}	A_{slab}	$\sqrt{A_{\text{slab}}}$	No. of transects	Groups of slabs
−0.236	−0.633	0.289	0.351	32	<660 km
−0.663	−0.74	−0.502	−0.562	44	=660 km
−0.466	−0.678	0.24	0.22	77	>660 km
−0.489	−0.697	−0.027	−0.022	153	All slabs
OPN	V_{up}	V_{sub}	V_{conv}	No. of transects	Groups of slabs
−0.221	−0.173	−0.065	0.062	32	<660 km
−0.709	0.413	0.47	0.373	44	=660 km
−0.513	−0.01	−0.185	−0.304	77	>660 km
−0.506	0.08	−0.022	−0.098	153	All slabs

Abbreviations: A_{re} = subduction duration since the latest initiation; A_{long} = subduction duration of the long-term age; A_{slab} = slab age; $\sqrt{A_{\text{slab}}}$ = square root of the slab age; *OPN* = overriding plate nature; V_{up} = the rate of upper plate motion; V_{sub} = subducting plate rate; V_{conv} = convergence rate.

Table 3
Multivariate Regression for Shallow Dip Angles

Model	Regression equation	*t* values of variables					R^2	R
		Intercept	First	Second	Third	Fourth		
S1	$\alpha_s = 33.4 - 0.0362 \times A_{\text{slab}} - 10.4 \times OPN$	20.3	−2.63	−7.80	—	—	0.289	0.538
S2	$\alpha_s = 31.9 - 0.0459 \times A_{re} - 7.21 \times OPN$	29.1	−5.29	−5.65	—	—	0.373	0.611
S3	$\alpha_s = 32.4 - 0.0596 \times A_{\text{long}} - 2.67 \times OPN$	33.4	−8.55	−2.00	—	—	0.500	0.707
S4	$\alpha_s = 36.6 - 0.0782 \times A_{\text{long}} - 0.0584 \times A_{\text{slab}}$	29.6	−14.1	−5.35	—	—	0.569	0.754
S5	$\alpha_s = 37.7 - 0.0579 \times A_{re} - 0.0612 \times A_{\text{slab}} - 8.35 \times OPN$	24.0	−6.84	−4.87	−6.90	—	0.459	0.677
S6	[a]$\alpha_s = 41.7 - 0.0702 \times A_{\text{long}} - 0.995 \times \sqrt{A_{\text{slab}}} - 3.14 \times OPN$	23.2	−10.7	−5.95	−2.60	—	0.596	0.772
S7	[a]$\alpha_s = 38.2 - 0.0681 \times A_{\text{long}} - 0.0618 \times A_{\text{slab}} - 3.44 \times OPN$	28.6	−10.5	−5.75	−2.83	—	0.591	0.769
S8	$\alpha_s = 37.4 - 0.0690 \times A_{\text{long}} - 0.0563 \times A_{\text{slab}} - 3.20 \times OPN + 0.334 \times V_{\text{sub}}$	26.3	−10.6	−4.95	−2.61	1.41	0.596	0.772
S9	$\alpha_s = 37.5 - 0.0690 \times A_{\text{long}} - 0.0605 \times A_{\text{slab}} - 3.27 \times OPN - 0.0748 \times V_{\text{up}}$	22.5	−10.3	−5.52	−2.61	−0.619	0.592	0.769
S10	$\alpha_s = 38.3 - 0.0678 \times A_{\text{long}} - 0.0618 \times A_{\text{slab}} - 3.49 \times OPN - 0.0272 \times V_{\text{conv}}$	21.9	−10.0	−5.73	−2.77	−0.147	0.591	0.769

Note. Parameters with *t* values >2.0 are significant.
[a]The preferred empirical model.

4.2. Multivariate Regression

In the previous section, we found the correlation between dip angles and other subduction parameters and identified the primary parameters that dominate variation of slab dip. However, slab dips are likely controlled by multiple parameters simultaneously (Jarrard, 1986). In this section, we follow the method of Jarrard (1986), applying multivariate regression to the data set, to investigate the combined effects of subduction parameters on slab dips (Tables 3 and 4). We use the python package *Statsmodels* (Seabold & Perktold, 2010) to carry out the multivariate regression.

For the shallow dip, the variation of dip angles can be best explained by the combination of subduction duration, slab age, and overriding plate nature, giving an R^2 value of 0.591 (Model S7 in Table 3) or 0.596 (Model S6 in Table 3) if the square root of slab age instead of its original value is considered. All these three variables are statistically significant based on *t* tests. Omitting any of the three variables causes an apparent drop in R^2, especially for subduction duration, which results in the largest drop in R^2 from 0.591 to 0.289 (Model S7 to S1 in Table 3). This implies that all three parameters contribute to the variation of shallow dips, while subduction duration is most significant. This result is consistent with the analysis in the previous section that shows a strong correlation between shallow dips and subduction duration (Figure 6). Compared to the reinitiation age, the long-term duration better explains the variation of shallow dip. For example, replacing the reinitiation age with long-term duration in the multiple regression that includes A_{slab} and *OPN* improves the correlation significantly, as evidenced by the increase of R^2 from 0.459 to 0.591 (Models S5 and S7 in Table 3).

Trade-off occurs between the long-term duration of subduction and the nature of the overriding plate. With slab age and *OPN*, the regression gives a *t* value of −7.80 for *OPN* (Model S1 in Table 3). When we add the long-term age to the regression, the *t* value of *OPN* drops to −2.83 (Model S7 in Table 3), suggesting a less significant *OPN*. In fact, *OPN* and the long-term age are correlated with a Pearson coefficient of 0.59, suggesting some collinearity between the two parameters. It is difficult to disentangle the contribution of *OPN* from that of the long-term age, but the latter is apparently more significant as shown by the stronger influence on R^2 and the largest *t* value. The three kinematic parameters, including convergence rate, subducting plate rate, and overriding plate motion, do not significantly contribute to the shallow dip variation. Adding any of the three parameters only marginally increases R^2, and a small *t* value suggests that these parameters are not statistically significant (Models S8–S10 in Table 3).

The analysis on the subduction zone-averaged data set confirms the earlier results (Table S3), including the dominant influence of subduction duration, especially the long-term age (Model X1 vs. X7); the significance of slab age (Model X4, X6, and X7); and the trade-off between the long-term duration of subduction and overriding plate nature (Model X1 vs. X7). One major difference between the two data sets is the significance level of overriding plate nature. For the subduction zone-averaged data set, overriding plate nature has *t*

Table 4
Multivariate Regression for the Deep Dips

Model	Regression equation	t values of variables						R^2	R
		Intercept	First	Second	Third	Fourth	Fifth		
D1	$\alpha_{d1} = 81.6 - 0.0937 \times A_{long} - 0.0256 \times A_{slab} - 2.59 \times OPN + 1.07 \times V_{up} - 2.84 \times V_{conv}$	21.5	−6.43	−1.01	−0.979	1.79	−5.58	0.529	0.727
D2	$\alpha_{d2} = 80.0 - 0.0337 \times A_{long} - 0.0483 \times A_{slab} - 3.99 \times OPN - 0.945 \times V_{up} - 1.94 \times V_{conv}$	15.3	−1.56	−1.38	−1.12	−1.11	−2.61	0.340	0.583
D3	$\alpha_{d3} = 85.1 + 0.0011 \times A_{long} - 0.0105 \times A_{slab} - 4.81 \times OPN + 0.339 \times V_{up} - 3.67 \times V_{conv}$	7.51	0.033	−0.230	−0.881	0.242	−2.77	0.224	0.473
D4	$\alpha_{d4} = 47.9 + 0.0238 \times A_{long} + 0.149 \times A_{slab} + 5.24 \times OPN + 1.27 \times V_{up} - 1.87 \times V_{conv}$	2.99	0.580	2.56	0.818	0.804	−1.15	0.215	0.464
D5	$\alpha_{d5} = 34.1 + 0.0631 \times A_{long} + 0.215 \times A_{slab} + 4.18 \times OPN - 2.68 \times V_{up} - 0.429 \times V_{conv}$	2.80	1.84	2.57	0.746	−2.15	−0.367	0.736	0.858
DP1	[a]$\alpha_{d1} = 79.0 - 0.0975 \times A_{long} + 1.36 \times V_{up} - 2.98 \times V_{conv}$	24.5	−9.01	2.60	−6.25	—	—	0.523	0.723
DP2	[a]$\alpha_{d2} = 77.0 - 0.0396 \times A_{long} - 2.48 \times V_{conv}$	21.2	−2.79	−5.07	—	—	—	0.312	0.559
DP3	[a]$\alpha_{d3} = 77.0 - 3.16 \times V_{conv}$	12.3	−3.96	—	—	—	—	0.207	0.455
DP4	[a]$\alpha_{d4} = 35.6 + 0.141 \times A_{slab} - 10.0 \times OPN$	5.86	3.22	2.19	—	—	—	0.187	0.432
DP4′	[a]$\alpha_{d4} = 27.9 + 2.22 \times \sqrt{A_{slab}} - 9.99 \times OPN$	3.34	3.10	2.17	—	—	—	0.176	0.420
DP5	[a]$\alpha_{d5} = 30.4 + 0.0857 \times A_{long} + 0.228 \times A_{slab} - 3.23 \times V_{up}$	4.47	3.74	6.11	−3.17	—	—	0.727	0.853
DP5′	[a]$\alpha_{d5} = 17.0 + 0.0895 \times A_{long} + 3.61 \times \sqrt{A_{slab}} - 3.10 \times V_{up}$	1.77	3.56	5.49	−2.84	—	—	0.692	0.832

Note. Parameters with t values >2.0 are significant.
[a]The preferred empirical model.

values <2.0, thus is not a significant parameter. However, we suggest that this is caused by the small sample size in this data set. With a sample size of 29 as opposed to 153 in the larger data set, all the t values are substantially reduced (Tables 3 and S3). Since the t values of overriding plate nature are close to 2.0, we still consider it as a significant parameter for the variation of the shallow dips.

Multivariate regression has been applied to the five deep dips (Table 4). We first include all the independent parameters in the regression equations, including long-term age of subduction duration, slab age, overriding plate nature, upper plate motion, and convergence rate. Overall, we observe a decreasing ability to explain these parameters as the depth increases, evidenced by the continuous drop in R^2 (Models D1–D4 in Table 4), except for the deepest dip (α_{d5}), which has a large R^2 of 0.736 (Model D5 in Table 4).

Through a systematic analysis where different parameter combinations are added and subtracted, we are able to find the preferred empirical model for deep dips (Table 4), which includes only the significant parameters with t values >2.0 while maximizing the R^2. We find that the long-term duration of subduction is a significant parameter for dips above 300 km, but its significance decreases with depth (Models DP1–DP3 in Table 4). Convergence rate is a significant parameter for dips above 400 km but becomes less significant as depth increases (Models DP1–DP4 in Table 4), similar to the long-term age of subduction duration. The combination of the two parameters explains most of the variation for dips above 400 km. The empirical relation becomes more complex for dips below 400 km. There is no clear trend at these depths.

4.3. Resolving the Contradiction

Interestingly, slab age does not correlate with shallow dips (A_{slab} or $\sqrt{A_{slab}}$) in our prior cross correlations, corroborating the analysis of Cruciani et al. (2005), but it is significant in multivariate regression. This seemingly contradictory conclusion can be reconciled by recognizing the influence that other parameters besides slab age have on slab dips. In this case, these parameters include subduction duration and overriding plate nature (Table 3). If we control the overriding plate nature variable and split the data into two categories

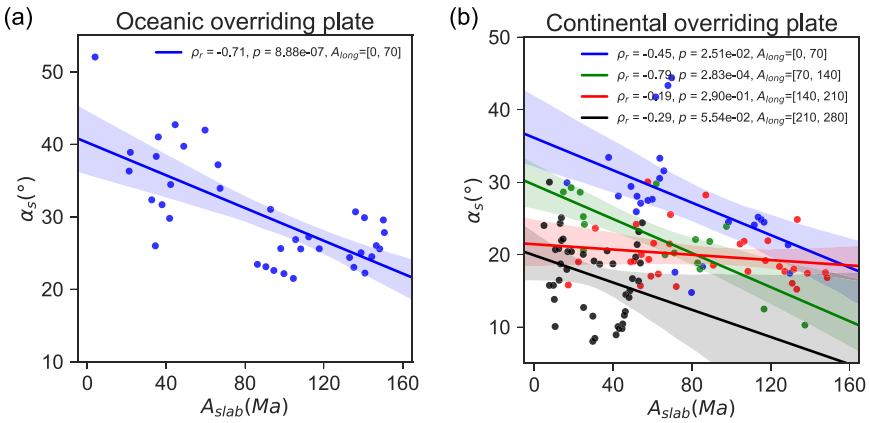

Figure 8. Correlation between shallow dip (α_s) and slab age (A_{slab}), for slabs with (a) oceanic overriding plates and (b) continental overriding plates. Different colors represent different age ranges of the long-term subduction duration. Pearson correlation (ρ_r) and p values are computed for each range of subduction duration.

(those with oceanic and those with continental overriding plates), we observe a strong correlation between shallow dips and slab age for slabs with oceanic overriding plates (Figure 8a). Although the dips within the group of continental overriding plate look quite random against slab age, once we split these data into groups with similar ages of subduction duration, some extent of correlation between shallow dips and slab age shows up as well (Figure 8b).

In fact, slab age does not correlate with shallow dips if those data are not categorized (Figure 6c), but it correlates moderately with the residual of the dips after the effects of subduction duration and overriding plate nature are removed (defined as $\alpha_s - C_{\text{long}} * A_{\text{long}} - C_{OPN} * OPN$, where C_{long} and C_{OPN} are the coefficients of the long-term subduction duration and overriding plate nature in the regression), with an R^2 value of −0.45 (Figure S5). These results demonstrate the power of multivariate regression in untangling the effects of multiple variables. We suggest that slab age is an essential factor in explaining the dip variation and that consistent negative coefficients (Figure 8) imply older slabs tend to have shallower dips.

5. Discussion

Subduction duration appears to be one of the most important parameters influencing slab dips. The significance of this parameter had been suggested with statistical analysis of 39 subduction segments (Jarrard, 1986) and geodynamic models (Gurnis & Hager, 1988) but has subsequently been largely overlooked. With a data set expanded to 153 transects and updated ages for subduction zones, we are able to confirm the strong influence of subduction duration on slab dips, while partly disentangling the influence of the long-term duration of subduction from the duration since last initiation of a subduction zone.

The physical mechanisms controlling slab dips are likely to be complex. Assuming a fixed trench and a rigid plate, analytical solutions suggest that the steady-state dip is controlled by the balance between the pressure gradient generated by mantle corner flow that tends to lift the slab and the negative buoyancy of the slab that tends to pull the slab downward (Stevenson & Turner, 1977). This method gives a slab dip of 63°, which is similar to the mean deep dips we found (50°–60°). Later, time-dependent numerical models with lower mantle subduction showed that slab dip can shallow with subduction duration, when trench migration relative to the mantle is allowed (Gurnis & Hager, 1988). This is likely due to the lateral migration of the slab to accommodate the difference in sinking rates between the lower viscosity upper mantle and the higher viscosity lower mantle (Billen, 2008). This lateral migration causes the slab hinge to move “ocean-ward” and the slab tip to move “continent-ward,” thus shallowing slab dip. Some regional geological reconstructions may support the shallowing of slab dip with subduction duration. For example, the westward migration of the magmatic arc in the Andean Cordillera since the Jurassic (Haschke et al., 2002) likely reflects the progressive shallowing of slab dips in this long-lasting subduction system.

We emphasize that the shallowing of slab with subduction duration is a long-term trend. Transient slab steepening could occur, for example, during the early stage of subduction before slab entering lower mantle (Funiciello et al., 2003), or as slab buckles (Guillaume et al., 2009). In addition, geodynamic models

(Gurnis & Hager, 1988) suggested that shallowing of slab with subduction duration occurred in a trench-retreat setting, which is also the dominant mode of trench migration at present. How slab dip evolves in a trench-advance setting still remains elusive. Our cross-correlation analysis suggests that shallowing of slab with subduction duration holds for trench-advance settings as well (Figure S4). However, the determination of trench migration mode depends strongly on the choice of absolute plate reference frames (Figure S6). Given the non-negligible discrepancies among existing reference frames, we remain cautious about this interpretation. We rely on future studies to more systematically investigate this question.

We find that the long-term age of subduction duration correlates better with slab dips than the reinitiation age (Figure 6), especially for the shallow dip that controls the overall dipping of a slab. This suggests that a short gap in subduction history does not fully reset the long-term state of the subduction system regionally. By regional state of the subduction system, we mean the rheological and density structure that it generally exhibits.

Several geodynamic processes could have been responsible for characterizing this long-term, regional state (Figure 10), including the tendency of subduction to continuously flux volatiles, melts, and cold slabs into the mantle. The interruption of subduction, through slab breakoff, ridge subduction, or changes in relative plate motion, leads to a gap in an otherwise contiguous slab. For example, Seton et al. (2015) suggest such a gap below East Asia: Subduction of the Izanagi-Pacific spreading center leads to a ca. 10 Myr hiatus in volcanism (Wu & Wu, 2019), evidence as a gap in high seismic velocities imaged with seismic tomography. A similar 10–15 Myr subduction hiatus could have also occurred beneath the Sundaland, as inferred from the magmatic gap between 75 and 60 Ma (McCourt et al., 1996) and the dynamic uplift and emergence of Sundaland between 80 and 60 Ma (Zahirovic et al., 2016). However, in these situations, the large-scale deeper source of negative buoyancy could still induce mantle flow that would tend to pull the new (reinitiated) slab in the direction of the overriding plate, making the new slab shallower. This force, from deep mantle flow, has been suggested to influence the flow beneath North America after the subduction of the Farallon plate (Zhou et al., 2018) and beneath Asia after the subduction of the Izanagi plate (Yang et al., 2019).

Dehydration of a slab could generate a large region of hydrated mantle over the long term (Figure 10), and this regional elevation in volatile concentrations is unlikely to dissipate immediately following an interruption in subduction. Since the creep strength of upper mantle assemblages is highly dependent on volatile concentrations (e.g., Hirth & Kohlstedt, 2003), these regions of high volatile concentrations are likely to be associated with regions of low effective viscosity. Indeed, such elevated volatile concentration is one mechanism that leads to the low viscosity of the mantle wedge required to fit gravity and topography above present-day slabs (Billen & Gurnis, 2001). The role that low viscosities play in controlling the changing dip of slabs is complicated (Manea & Gurnis, 2007; van Hunen et al., 2004). With time-dependent geodynamic models, Manea and Gurnis (2007) found two divergent evolutionary pathways depending on the depth extent of a region of lowered viscosity. If the lowered viscosities extend through the upper mantle, the tendency is to maintain a steeply dipping slab, while confinement of lower viscosities to just below the lithosphere (e.g., above about 200 km depth) tends to produce slabs that are shallowly dipping beneath the overriding plate. The tendency of slabs to shallow in the longer term suggests that hydration and hence weakening might be confined to shallower depths.

Finally, the long-term evolution of the subduction shear zone at the plate interface may also contribute to slab shallowing (Figure 10). A decreasing viscosity in the shear zone due to grain-size reduction (Etheridge & Wilkie, 1979; Foley & Bercovici, 2014) and slab dehydration, and the shallowing of the shear zone with the duration of subduction, could reduce the viscous resistance between the slab and overriding plate, favoring the formation of a shallow-dipping slab (Manea & Gurnis, 2007).

The tendency for slab dips to shallow with subduction duration has important implications for the study of flat slabs. A variety of mechanisms have been proposed to cause flat slabs, such as enhanced hydrodynamic suction in the mantle wedge due to thick overriding plate (e.g., Jones et al., 2011; Rodríguez-González et al., 2012), increased chemical buoyancy of a subducting slab due to oceanic plateaus (e.g., Gutscher et al., 2000; Hu et al., 2016; Liu et al., 2010), the fast trenchward motion of the overriding plate (van Hunen et al., 2000), and a low-strength channel between the slab and overriding plate (Manea & Gurnis, 2007). However, a systematic study on the relation between flat slab and subduction duration has not been carried out. Empirically, most flat slabs have occurred in old subduction systems (around 100 Myr or longer), including the Peru, Central Chile, Central Mexico, and Southern Alaska flat slabs at present, as well as the Farallon

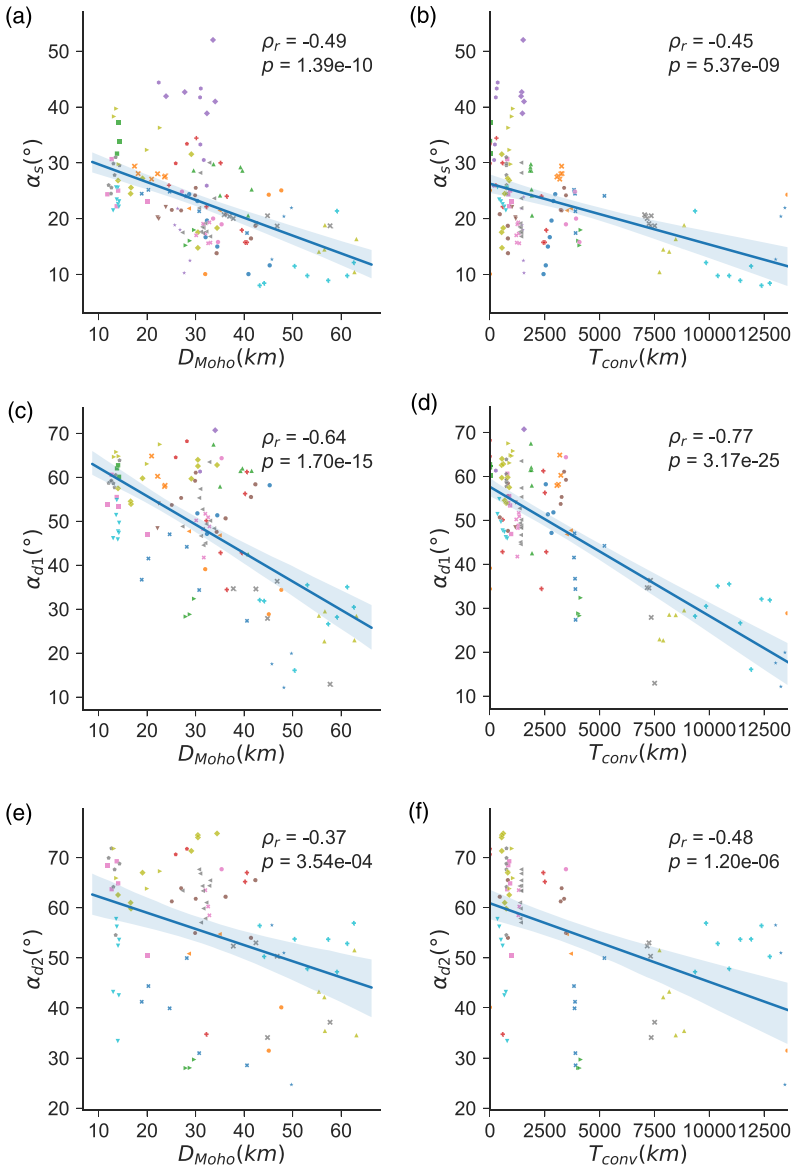

Figure 9. Correlation between slab dips and subduction parameters including maximum Moho depth (a, c, e) and total convergence (b, d, f). Other annotations are the same as in Figure 6.

flat slab in the past. This seems to suggest that a long subduction history could be necessary in the onset of flat slab subduction.

Our analysis has also revealed the importance of overriding plate nature in predicting slab dips, especially for shallow dips (Table 2), consistent with earlier studies (e.g., Furlong et al., 1982; Jarrard, 1986; Holt et al., 2015; Lallemand et al., 2005). Geodynamic models suggest that a thick overriding plate could even cause the slab to be flat as an extreme case, thus favoring the continental plate over oceanic plate in forming shallow slabs (Hu et al., 2016; Kukacka, 2004; Rodríguez-González et al., 2012). In order to verify this concept, we have compiled maximum Moho depth within 300 km from the trench for each transect. With this continuous variable, we are able to better demonstrate the relationship between slab dip and the thickness of overriding plate. We find that the maximum Moho depth correlates well with the slab dips above 200 km (Figure 9), confirming the significance of overriding plate nature in explaining the variation of slab dips. Replacing the *OPN* with maximum Moho depth in the regression equation of shallow dip gives an R^2 of 0.592, similar to the original value of 0.591. This suggests that the available data set does not have the power to resolve a more

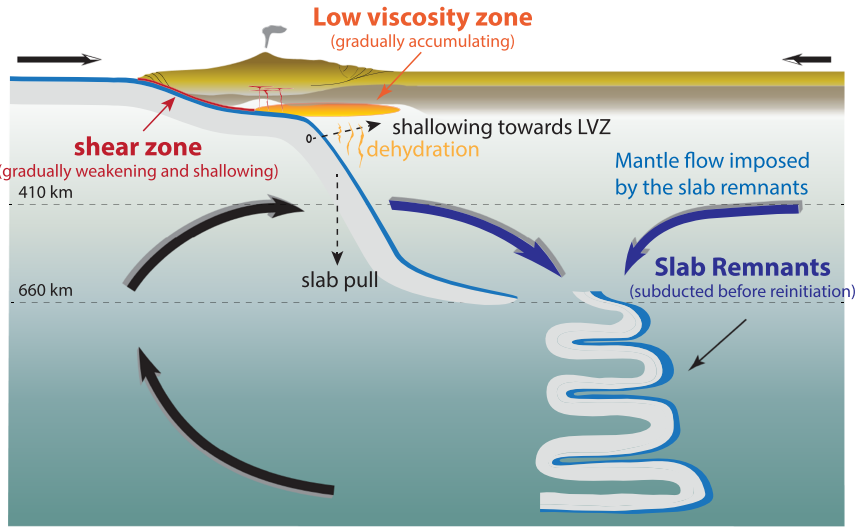

Figure 10. Long-term state of the subduction zone, where the slab remnants (from earlier subduction), the low viscosity zone at shallow depth, and the shear zone at the plate interface inherited from earlier subduction contribute to the shallowing of the new slab.

sophisticated relationship between slab dips and overriding plate. A simple dummy variable *OPN* is able to capture most of the variation caused by the nature of overriding plate.

In our analysis, upper plate motion is not correlated with the shallow dip (Figure 7). Even if different groups of slabs classified by their maximum depth are considered, the correlation remains weak (Table 2). In contrast, Lallemand et al. (2005) observed a much stronger correlation, especially for slabs that penetrate into the lower mantle. This is likely caused by several reasons. First, the two studies have obtained contrasting values of maximum slab depth for some subduction zones, which leads to subduction zones falling into different depth categories. For example, in Lallemand et al. (2005), the Tonga slab is categorized into the =660 group, while the Middle American slab into the <660 group. However, in our data set, Tonga slab and Middle American slab both extend into the lower mantle. This has been confirmed by recent seismic tomography models (e.g., Li et al., 2008; Obayashi et al., 2013; Simmons et al., 2012). Second, Lallemand et al. (2005) excluded near-edge transects with which the trend was likely less clear, while we have kept those transects.

Finally, the trench-normal component of upper plate motion is sensitive to the choice of absolute reference frames. Lallemand et al. (2005) used a hotspot reference frame (Gripp & Gordon, 2002), while our data are based on a moving Indian/Atlantic hotspot reference frame (O'Neill et al., 2005). This could have caused a significant difference in the rate of upper plate motion, considering that overriding plates usually have small velocities (Figure S6). From the statistical point of view, we suggest that the correlation between the shallow dip and upper plate motion may exist but requires specific conditions, such as certain reference frame and certain category of slabs. Meanwhile, numerical (Arcay et al., 2008) and laboratory (Heuret et al., 2007) experiments have also suggested that upper plate advance toward the trench tends to cause shallower dips than upper plate retreat, although the motion of the upper plate is prescribed in these models instead of as a natural response to subduction. We suggest that upper plate motion is likely an important parameter, but further investigation is still needed.

We find that slab age contributes to shallow dips, where older slabs tend to have steeper dips. Our analysis reveals a very weak correlation between the shallow dip and slab age or the squared root of slab age. However, we found this simple cross-correlation analysis deceptive. Multivariate regression suggests that slab age is a significant variable (Table 3). This is further confirmed by the greatly improved correlation once we categorize the shallow dips based on overriding plate nature and subduction duration (Figure 8). Theoretically, increasing slab age will increase the negative buoyancy of slab, resulting in larger slab pull force and a steeper slab. However, this effect could be counterbalanced by other factors. For example, the elastic and viscous resistance to slab bending is proportional to the cube of the elastic and viscous thickness of the slab, respectively, which increase with slab age (Conrad & Hager, 1999; Turcotte & Schubert, 1982). The resisting

forces make it difficult to bend the slab for old slabs, which counterbalances the thermal buoyancy. In addition, Conrad et al. (2004) suggested that the slab negative buoyancy transmitted to the surface plate varied with the depth of plate-slab coupling, which depended on the stress environment of the subduction zones. The multivariate regression suggests that with these complex mechanisms combined, the resistance to slab bending outmatches the negative buoyancy for old slabs, causing the shallowing of slab dips. This conclusion is consistent with laboratory (Bellahsen et al., 2005) and numerical (Holt et al., 2015; Hu et al., 2016) studies that show a reduced slab dip or increased radius of subducting plate curvature for older slabs.

Convergence rate is poorly correlated with the shallow dip (Figure 6). Multivariate regression suggests that it does not contribute to the variation of the shallow dip as adding this parameter does not lead to any increase in R^2 values (Table 3). This is consistent with the result of Jarrard (1986). In contrast, we find that the total convergence throughout the subduction history is moderately correlated with the shallow dip, with a Pearson correlation coefficient of −0.45 (Figure 9), which is understandable because the shallow dip correlates strongly with subduction duration, and subduction duration correlates strongly with total convergence. This further suggests that subduction duration is more important in determining the shallow dip. However, a moderate correlation exists between convergence rate and deep dips (Figure 7). Multiple regression also suggests that it is a significant variable for dips between 100 and 400 km (Table 4).

The depth dependence of the relationship between dip and other subduction parameters has been largely overlooked in earlier studies, but we suggest that it is robust. Except for the convergence rate, the effect of subduction duration is also depth dependent (Figure 7 and Table 4). There is a clear trend such that the influence of subduction duration decreases with depth for dips above 500 km. In addition, the overall ability of the subduction parameters to explain the observed variance decreases with depth (Models D1–D4 in Table 4). This is likely because the influence from mantle flow becomes stronger as the depth increases. The large R^2 for α_{d5} is puzzling (Model D5 in Table 4). It is not likely a robust result because of the small sample size, $N = 31$ (Figure 4). We realize that substantial uncertainties exist in the analysis of deep dips, due to the limited sample size, especially for dips below 300 km. Similarly, we also observed the dependence of the relationship between dip and other subduction parameters on the maximum length of the slab (Table 2), consistent with Lallemand et al. (2005). That depth-dependent relationship is intriguing and has to be further tested by numerical and analog models.

6. Conclusion

We have compiled slab dip angles along with subduction parameters, including subduction duration, slab age, overriding plate nature, convergence rate, subducting plate rate, and upper plate motion, along major subduction zones. Based on our cross-correlation analysis and multivariate regression, we are able to confirm the following concepts:

1. Subduction duration is one of the most significant parameters in determining the dip angle of a slab. Older subduction systems tend to have shallower dips. Long-term duration of subduction correlates better with the shallow dip than the reinitiation age, suggesting the importance of the long-term state of a subduction zone (Figure 10).
2. Overriding plate nature is an influential parameter for the shallow dip, while convergence rate can affect deep dips above 400 km.
3. Slab age negatively correlates with the shallow dip, especially for subduction zones with oceanic overriding plates, suggesting that older slabs tend to have shallower dips.
4. The relationship between slab dips and subduction parameters is depth dependent. The ability to explain slab dip using subduction duration and overriding plate nature decreases with depth.

Acknowledgments
We acknowledge the support from the National Science Foundation under EAR-1645775. We thank Adam Holt and two anonymous reviewers for their helpful comments on an earlier version of our manuscript. The subduction parameters are compiled using PyGPlates (http://www.gplates.org/docs.html). All data used in the current study are available in the online version of the paper. Data from this study can also be found on CaltechDATA (doi:10.22002/D1.1380).

References

Amato, J., & Pavlis, T. (2010). Chugach terrane, southern Alaska, reveal multiple episodes of accretion and erosion in a subduction complex. *Geology*, *38*, 459–462. https://doi.org/10.1130/G30719.1

Arcay, D., Lallemand, S., & Doin, M.-P. (2008). Back-arc strain in subduction zones: Statistical observations versus numerical modeling. *Geochemistry, Geophysics, Geosystems*, *9*, Q05015. https://doi.org/10.1029/2007GC001875

Arculus, R., Gurnis, M., Ishizuka, O., Reagan, M.-K., Pearce, J., & Sutherland, R. (2019). How to create new subduction zones: A global perspective. *Oceanography*, *32*, 160–174. https://doi.org/10.5670/oceanog.2019.140

Ballance, P.-F., Ablaev, A.-G., Pushchin, I.-K., Pletnev, S.-P., Birylina, M.-G., Itaya, T., et al. (1999). Morphology and history of the Kermadec trench–arc–backarc basin–remnant arc system at 30 to 32°S: Geophysical profile, microfossil and K–Ar data. *Marine Geology*, *159*(1-4), 35–62.

Barker, P.-F. (2001). Scotia Sea regional tectonic evolution: Implications for mantle flow and palaeocirculation. *Earth-Science Reviews*, *55*(1-2), 1–39. https://doi.org/10.1016/s0012-8252(01)00055-1

Bellahsen, N., Faccenna, C., & Funiciello, F. (2005). Dynamics of subduction and plate motion in laboratory experiments: Insights into the "plate tectonics" behavior of the Earth. *Journal of Geophysical Research*, *110*, B01401. https://doi.org/10.1029/2004JB002999

Billen, M. (2008). Modeling the dynamics of subducting slabs. *Annual Review of Earth and Planetary Sciences*, *36*(1), 325–356. https://doi.org/10.1146/annurev.earth.36.031207.124129

Billen, M., & Gurnis, M. (2001). A low viscosity wedge in subduction zones. *Earth and Planetary Science Letters*, *193*, 227–236. https://doi.org/10.1016/S0012-821X(01)00482-4

Bond, G. (1973). A late Paleozoic volcanic arc in the eastern Alaska Range. *The Journal of Geology*, *81*, 557–575.

Boschman, L., van Hinsbergen, D., Kimbrough, D., Langereis, C., & Spakman, W. (2018). The dynamic history of 220 million years of subduction below Mexico: A correlation between slab geometry and overriding plate deformation based on geology, paleomagnetism, and seismic tomography. *Geochemistry, Geophysics, Geosystems*, *19*, 4649–4672. https://doi.org/10.1029/2018GC007739

Boschman, L., van Hinsbergen, D., Torsvik, T., Spakman, W., & Pindell, J. (2014). Kinematic reconstruction of the Caribbean region since the Early Jurassic. *Earth-Science Reviews*, *138*, 102–136. https://doi.org/10.1016/j.earscirev.2014.08.007

Briden, J., Rex, D., Faller, A., & Tomblin, J. (1979). K-Ar geochronology and paleomagnatism of volcanic rocks in the Lesser Antilles island arc. *Philosophical Transactions of the Royal Society of London. Series A: Mathematical and Physical Sciences*, *291*, 485–528.

Buchs, D., Arculus, R., Baumgartner, P., Baumgartner-Mora, C., & Ulianov, A. (2010). Late Cretaceous arc development on the SW margin of the Caribbean Plate: Insights from the Golfito, Costa Rica, and Azuero, Panama. *Geochemistry, Geophysics, Geosystems*, *11*, Q07S24. https://doi.org/10.1029/2009GC002901

Chen, Y., Wu, J., & Suppe, J. (2019). Southward propagation of Nazca subduction along the Andes. *Nature*, *565*, 441–447. https://doi.org/10.1038/s41586-018-0860-1

Clements, B., & Hall, R. (2011). A record of continental collision and regional sediment flux for the Cretaceous and Palaeogene core of SE Asia: Implications for early Cenozoic palaeogeography. *Journal of the Geological Society*, *168*, 1187–1200. https://doi.org/10.1144/0016-76492011-004

Conrad, C.-P., Bilek, S., & Lithgow-Bertelloni, C. (2004). Great earthquakes and slab pull: Interaction between seismic coupling and plate–slab coupling. *Earth and Planetary Science Letters*, *218*(1-2), 109–122.

Conrad, C.-P., & Hager, B.-H. (1999). Effects of plate bending and fault strength at subduction zones on plate dynamics. *Journal of Geophysical Research*, *104*, 17,551–17,571.

Cooper, P., & Taylor, B. (1985). Polarity reversal in the Solomon Island arc. *Nature*, *314*, 428–430.

Cruciani, C., Carminati, E., & Doglioni, C. (2005). Slab dip vs. lithosphere age: No direct function. *Earth and Planetary Science Letters*, *238*(3-4), 298–310. https://doi.org/10.1016/j.epsl.2005.07.025

Dickinson, W.-R. (1973). Widths of modern arc-trench gaps proportional to past duration of igneous activity in associated magmatic arcs. *Journal of Geophysical Research*, *78*(17), 3376–3389. https://doi.org/10.1029/jb078i017p03376

Doglioni, C., Harabaglia, P., Merlini, S., Mongelli, F., Peccerillo, A., & Piromallo, C. (1999). Orogens and slabs vs. their direction of subduction. *Earth-Science Reviews*, *45*(3-4), 167–208. https://doi.org/10.1016/s0012-8252(98)00045-2

Domeier, M., & Torsvik, T. (2014). Plate tectonics in the late Paleozoic. *Geoscience Frontiers*, *5*, 303–350.

Etheridge, M., & Wilkie, J. (1979). Grainsize reduction, grain boundary sliding and the flow strength of mylonites. *Tectonophysics*, *58*(1-2), 159–178.

Flament, N., Gurnis, M., Williams, S., Seton, M., Skogseid, J., Heine, C., & Müller, R. (2014). Topographic asymmetry of the South Atlantic from global models of mantle flow and lithospheric stretching. *Earth and Planetary Science Letters*, *387*, 107–119. https://doi.org/10.1016/j.epsl.2013.11.017

Foley, B.-J., & Bercovici, D. (2014). Scaling laws for convection with temperature-dependent viscosity and grain-damage. *Geophysical Journal International*, *199*(1), 580–603.

Funiciello, F., Faccenna, C., Giardini, D., & Regenauer-Lieb, K. (2003). Dynamics of retreating slabs: 2. Insights from three-dimensional laboratory experiments. *Journal of Geophysical Research*, *108*(B4), 2207. https://doi.org/10.1029/2001JB000896

Furlong, K.-P., Chapman, D.-S., & Alfeld, P.-W. (1982). Thermal modeling of the geometry of subduction with implications for the tectonics of the overriding plate. *Journal of Geophysical Research*, *87*(B3), 1786–1802.

Greene, H., Collot, J.-Y., Fisher, M., & Crawford, A. (1994). Neogene tectonic evolution of the New Hebrides island arc: A review incorporating ODP drilling results. In *Proceedings of the Ocean Drilling Program, Scientific Results* (Vol. 134, pp. 19–46). College Station, TX: Ocean Drilling Program. https://doi.org/10.2973/odp.proc.sr.134.002.1994

Gripp, A.-E., & Gordon, R.-G. (2002). Young tracks of hotspots and current plate velocities. *Geophysical Journal International*, *150*(2), 321–361.

Guillaume, B., Martinod, J., & Espurt, N. (2009). Variations of slab dip and overriding plate tectonics during subduction: Insights from analogue modelling. *Tectonophysics*, *463*, 167–174. https://doi.org/10.1016/j.tecto.2008.09.043

Gurnis, M., & Hager, B.-H. (1988). Controls of the structure of subducted slabs. *Nature*, *335*(6188), 317–321. https://doi.org/10.1038/335317a0

Gurnis, M., Hall, C., & Lavier, L. (2004). Evolving force balance during incipient subduction. *Geochemistry, Geophysics, Geosystems*, *5*, Q07001. https://doi.org/10.1029/2003gc000681

Gurnis, M., Van Avendonk, H., Gulick, S., Stock, J., Sutherland, R., Hightower, E., et al. (2019). Incipient subduction at the contact with stretched continental crust: The Puysegur Trench. *Earth and Planetary Science Letters*, *517*, 212–219. https://doi.org/10.1016/j.epsl.2019.04.025

Gutscher, M.-A., Spakman, W., Bijwaard, H., & Engdahl, E.-R. (2000). Geodynamics of flat subduction: Seismicity and tomographic constraints from the Andean margin. *Tectonics*, *19*(5), 814–833.

Hall, R. (2018). The subduction initiation stage of the Wilson cycle. *Geological Society, London, Special Publications*, 470(1), 415–437. https://doi.org/10.1144/SP470.3

Hamilton, W.-B. (1979). Tectonics of the Indonesian region. US Geological Survey. https://doi.org/10.3133/pp1078

Haschke, M., Siebel, W., Günther, A., & Scheuber, E. (2002). Repeated crustal thickening and recycling during the Andean orogeny in north Chile (21°–26°S). *Journal of Geophysical Research*, *107*(B1), 2019. https://doi.org/10.1029/2001JB000328

Hayes, G.-P., Moore, G.-L., Portner, D.-E., Hearne, M., Flamme, H., Furtney, M., & Smoczyk, G.-M. (2018). Slab2, a comprehensive subduction zone geometry model. *Science*, *362*(6410), 58–61.

Heuret, A., Funiciello, F., Faccenna, C., & Lallemand, S. (2007). Plate kinematics, slab shape and back-arc stress: A comparison between laboratory models and current subduction zones. *Earth and Planetary Science Letters*, *256*(3-4), 473–483. https://doi.org/10.1016/j.epsl.2007.02.004

Hirth, G., & Kohlstedt, D. (2003). Rheology of the upper mantle and the mantle wedge: A view from the experimentalists. In J. Eiler (Ed.), *Inside the subduction factory* (pp. 83–105). Washington, DC: American Geophysical Union.

Hoernle, K., Höfig, T., Bezard, R., Portnyagin, M., Hauff, F., Wartho, J., et al. (2018). New insights into the formation and evolution of the Aleutian arc. In *Abstract T13-04 presented at 2018 Fall Meeting, 10–14 December*. AGU: Washington, DC.

Holt, A.-F., Buffett, B.-A., & Becker, T.-W. (2015). Overriding plate thickness control on subducting plate curvature. *Geophysical Research Letters*, *42*, 3802–3810. https://doi.org/10.1002/2015GL063834

Horton, B., & Fuentes, F. (2016). Sedimentary record of plate coupling and decoupling during growth of the Andes. *Geology*, *44*, 647–650. https://doi.org/10.1130/G37918.1

House, M., Gurnis, M., Kamp, P., & Sutherland, R. (2002). Uplift in the Fiordland region, New Zealand: Implications for incipient subduction. *Science*, *297*(5589), 2038–2041.

House, M., Gurnis, M., Sutherland, R., & Kamp, P. (2005). Patterns of Late Cenozoic exhumation deduced from apatite and zircon U-He ages from Fiordland, New Zealand. *Geochemistry, Geophysics, Geosystems*, *6*, Q09013. https://doi.org/10.1029/2005gc000968

Hu, J., & Liu, L. (2016). Abnormal seismological and magmatic processes controlled by the tearing South American flat slabs. *Earth and Planetary Science Letters*, *450*, 40–51.

Hu, J., Liu, L., Hermosillo, A., & Zhou, Q. (2016). Simulation of late Cenozoic South American flat-slab subduction using geodynamic models with data assimilation. *Earth and Planetary Science Letters*, *438*, 1–13.

Ishizuka, O., Hickey-Vargas, R., Arculus, R., Yogodzinski, G., Savov, I., Kusano, Y., et al. (2018). Age of Izu-Bonin-Mariana arc basement. *Earth and Planetary Science Letters*, *481*, 80–90. https://doi.org/10.1016/j.epsl.2017.10.023

Ishizuka, O., Tani, K., Reagan, M., Kanayama, K., Umino, S., Harigane, Y., et al. (2011). Timescales of subduction initiation and subsequent evolution of an oceanic island arc. *Earth and Planetary Science Letters*, *306*, 229–240. https://doi.org/10.1016/j.epsl.2011.04.006

Jarrard, R.-D. (1986). Relations among subduction parameters. *Reviews of Geophysics*, *24*(2), 217–284.

Jego, S., Maury, R., Polve, M., Yumul, G., Bellon, R., Hand Tamayo., & Cotten, J. (2005). Geochemistry of adakites from the Philippines: Constraints on their origins. *Resource Geology*, *55*, 163–187.

Jicha, B., Scholl, D., Singer, B., Yogodzinski, G., & Kay, S. (2006). Revised age of Aleutian island arc formation implies high rate of magma production. *Geology*, *34*, 661–664. https://doi.org/10.1130/G22433.1

Jones, C.-H., Farmer, G.-L., Sageman, B., & Zhong, S. (2011). Hydrodynamic mechanism for the Laramide orogeny. *Geosphere*, *7*(1), 183–201.

Keenan, T., Encarnación, J., Buchwaldt, R., Fernandez, D., Mattinson, J., Rasoazanamparany, C., & Luetkemeyer, P. (2016). Rapid conversion of an oceanic spreading center to a subduction zone inferred from high-precision geochronology. *Proceedings of the National Academy of Sciences of the United States of America*, *113*, E7359–E7366. https://doi.org/10.1073/pnas.1609999113

Kimura, J.-I., Stern, R.-J., & Yoshida, T. (2005). Reinitiation of subduction and magmatic responses in SW Japan during Neogene time. *Geological Society of America Bulletin*, *117*(7), 969. https://doi.org/10.1130/b25565.1

Kukacka, M. (2004). Influence of the zone of weakness on dip angle and shear heating of subducted slabs. *Physics of The Earth and Planetary Interiors*, *141*(4), 243–252. https://doi.org/10.1016/j.pepi.2003.11.004

Lallemand, S., Heuret, A., & Boutelier, D. (2005). On the relationships between slab dip, back-arc stress, upper plate absolute motion, and crustal nature in subduction zones. *Geochemistry, Geophysics, Geosystems*, *6*, Q09006. https://doi.org/10.1029/2005GC000917

Laske, G., Masters, G., Ma, Z., & Pasyanos, M. (2013). Update on CRUST1. 0—A 1-degree global model of Earth's crust. In *Geophys. Res. Abstr* (Vol. 15, pp. 2658). Vienna, Australia: EGU General Assembly.

Leng, W., & Gurnis, M. (2015). Subduction initiation at relic arcs. *Geophysical Research Letters*, *42*, 7014–7021. https://doi.org/10.1002/2015GL064985

Li, C., Van Der Hilst, R.-D., Engdahl, E.-R., & Burdick, S. (2008). A new global model for P wave speed variations in Earth's mantle. *Geochemistry, Geophysics, Geosystems*, *9*, Q05018. https://doi.org/10.1029/2007GC001806

Lindley, I. (2006). Extension and vertical tectonics in the New Guinea islands: Implications for island arc evolution. *Annals of Geophysics Supply*, *49*, 403–426.

Liu, L., Gurnis, M., Seton, M., Saleeby, J., Müller, R.-D., & Jackson, J.-M. (2010). The role of oceanic plateau subduction in the Laramide orogeny. *Nature Geoscience*, *3*(5), 353.

Ma, P., Liu, S., Gurnis, M., & Zhang, B. (2019). Slab horizontal subduction and slab tearing beneath East Asia. *Geophysical Research Letters*, *46*, 5161–5169. https://doi.org/10.1029/2018GL081703

Macfarlane, A., Carney, J., Crawford, A., & Greene, H. (1988). Vanuatu—A review of the onshore geology, Geology and offshore resources of Pacific island arcs - Vanuatu region. *Circum-Pacific Council for Energy and Mineral Resources*, 8, pp. 45–91.

Manea, V., & Gurnis, M. (2007). Subduction zone evolution and low viscosity wedges and channels. *Earth and Planetary Science Letters*, *264*(1-2), 22–45.

McCourt, W., Crow, M., Cobbing, E., & Amin, T. (1996). Mesozoic and Cenozoic plutonic evolution of SE Asia: Evidence from Sumatra, Indonesia. *Geological Society, London, Special Publications*, *106*, 321–335. https://doi.org/10.1144/GSL.SP.1996.106.01.21

McDougall, I. (1994). Dating of rhyolitic glass in the Tonga forearc (Hole 841B). In *Proceedings of the Ocean Drilling Program. Scientific Results* (Vol. 135, pp. 923). College Station, TX: Ocean Drilling Program.

Meffre, S., Falloon, T., Crawford, T., Hoernle, K., Hauff, F., Duncan, R., et al. (2012). Basalts erupted along the Tongan fore arc during subduction initiation: Evidence from geochronology of dredged rocks from the Tonga fore arc and trench. *Geochemistry, Geophysics, Geosystems*, *13*, Q12003. https://doi.org/10.1029/2012GC004335

Miyazaki, K., Ozaki, M., Saito, M., & Toshimitsu, S. (2016). The kyushu–ryukyu arc. In T. Moreno, T. Kojima, & W. Gibbons (Eds.), *Geology of Japan* (pp. 1–24). London: Geol. Soc.

Moore, G.-W. (1973). Westward tidal lag as the driving force of plate tectonics. *Geology*, *1*(3), 99–100.

Mortimer, N., Gans, P., Foley, F., Turner, M., Daczko, N., Robertson, M., & Turnbull, I. (2013). Geology and age of Solander Volcano, Fiordland, New Zealand. *Journal of Geology*, *121*, 475–487. https://doi.org/10.1086/671397

Mortimer, N., Gans, P., Meffre, S., Martin, C., Seton, M., Williams, S., et al. (2018). Regional volcanism of northern Zealandia: Post-Gondwana break-up magmatism on an extended, submerged continent. *Geological Society, London, Special Publications*, 463(1), 199–226.

Mpodozis, C., & Ramos, V. (1989). The Andes of Chile and Argentina. In G. Ericksen, M. Cañas Pinochet, & J. Reinemud (Eds.), *Geology of the Andes and its relation to hydrocarbon and mineral resources* (pp. 59–90). Houston, TX: Circum-Pacific Council for Energy and Mineral Resources.

Mukasa, S., & Dalziel, I. (1996). Southernmost Andes and South Georgia Island, North Scotia Ridge: Zircon U-Pb and $^{40}Ar/^{39}Ar$ muscovite age constraints on tectonic evolution of Southwestern Gondwanaland. *Journal of South American Earth Sciences*, *9*, 349–365.

Müller, R.-D., Roest, W.-R., Royer, J.-Y., Gahagan, L.-M., & Sclater, J.-G. (1997). Digital isochrons of the world's ocean floor. *Journal of Geophysical Research*, *102*(B2), 3211–3214.

Müller, R.-D., Sdrolias, M., Gaina, C., & Roest, W.-R. (2008). Age, spreading rates, and spreading asymmetry of the world's ocean crust. *Geochemistry, Geophysics, Geosystems*, *9*, Q04006. https://doi.org/10.1029/2007GC001743

Müller, R.-D., Seton, M., Zahirovic, S., Williams, S.-E., Matthews, K.-J., Wright, N.-M., et al. (2016). Ocean basin evolution and global-scale plate reorganization events since Pangea breakup. *Annual Review of Earth and Planetary Sciences*, *44*(1), 107–138. https://doi.org/10.1146/annurev-earth-060115-012211

Neill, I., Kerr, A., Hastie, A., Stanek, K., & Millar, I. (2011). Origin of the Aves Ridge and Dutch–Venezuelan Antilles: Interaction of the Cretaceous 'Great Arc' and Caribbean-Colombian Oceanic Plateau. *Journal of the Geological Society*, *168*, 333–348. https://doi.org/10.1144/0016-76492010-067

O'Neill, C., Müller, D., & Steinberger, B. (2005). On the uncertainties in hot spot reconstructions and the significance of moving hot spot reference frames. *Geochemistry, Geophysics, Geosystems*, *6*, Q04003. https://doi.org/10.1029/2004GC000784

Obayashi, M., Yoshimitsu, J., Nolet, G., Fukao, Y., Shiobara, H., Sugioka, H., et al. (2013). Finite frequency whole mantle P wave tomography: Improvement of subducted slab images. *Geophysical Research Letters*, *40*, 5652–5657. https://doi.org/10.1002/2013GL057401

Pearson, K. (1895). Notes on regression and inheritance in the iCase of two parents. *Proceedings of the Royal Society of London*, *58*, 240–242.

Pedersen, R., Searle, M., Carter, A., & Bandopadhyay, P. (2010). U-Pb zircon age of the Andaman ophiolite: Implications for the beginning of subduction beneath the Andaman-Sumatra arc. *Journal of the Geological Society*, *167*, 1105–1112. https://doi.org/10.1144/0016-76492009-151

Pelletier, B., Lafoy, Y., & Missegue, F. (1993). Morphostructure and magnetic fabric of the northwestern North Fiji Basin. *Geophysical Research Letters*, *20*, 1151–1154. https://doi.org/10.1029/93GL01240

Petterson, M., Babbs, T., Neal, C., Mahoney, J., Saunders, A., Duncan, R., et al. (1999). Geological–tectonic framework of Solomon Islands, SW Pacific: Crustal accretion and growth within an intra-oceanic setting. *Tectonophysics*, *301*(1-2), 35–60. https://doi.org/10.1016/s0040-1951(98)00214-5

Plafker, G., Nokleberg, W., & Lull, J. (1989). Bedrock geology and tectonic evolution of the Wrangellia, Peninsular, and Chugach terranes along the Trans-Alaska Crustal Transect in the northern Chugach Mountains and southern Copper River Basin, Alaska. *Journal of Geophysical Research*, *94*, 4255–4295. https://doi.org/10.1029/JB094iB04p04255

Ramos, V., & Folguera, A. (2009). Andean flat-slab subduction through time. *Geological Society, London, Special Publications*, *327*, 31–54.

Reagan, M., Ishizuka, I., Stern, R., Kelley, K., Ohara, Y., Blichert-Toft, J., et al. (2010). Fore-arc basalts and subduction initiation in the Izu-Bonin-Mariana system. *Geochemistry, Geophysics, Geosystems*, *11*, Q03X12. https://doi.org/10.1029/2009GC002871

Rioux, M., Hacker, B., Mattinson, J., Kelemen, P., Blusztajn, J., & Gehrels, G. (2007). High-precision U-Pb zircon and whole-rock isotopic analyses from the accreted Talkeetna arc, south-central Alaska. *Geological Society of America Bulletin*, *119*, 1168–1184. https://doi.org/10.1130/B25964.1

Rodríguez-González, J., Negredo, A., & Billen, M. (2012). The role of the overriding plate thermal state on slab dip variability and on the occurrence of flat subduction. *Geochemistry, Geophysics, Geosystems*, *13*, Q01002. https://doi.org/10.1029/2011gc003859

Saleeby, J. (2011). Geochemical mapping of the Kiings-Kaweah ophiolite belt, California—Evidence for progressive mélange formation in a large offset transform subduction initiation environment. In *Mélanges: Processes of Formation and Societal Significance*, Geological Society of America Special Paper (Vol. 480, pp. 31–73). https://doi.org/10.1130/2011.2480(02)

Schellart, W. (2007). The potential influence of subduction zone polarity on overriding plate deformation, trench migration and slab dip angle. *Tectonophysics*, *445*(3-4), 363–372. https://doi.org/10.1016/j.tecto.2007.09.009

Schellart, W. (2017). Andean mountain building and magmatic arc migration driven by subduction-induced whole mantle flow. *Nature Communications*, *8*(1), 2010. https://doi.org/10.1038/s41467-017-01847-z

Schellart, W., Lister, G., Sussman, A., & Weil, A. (2004). Tectonic models for the formation of arc-shaped convergent zones and backarc basins. In *Orogenic curvature: Integrating paleomagnetic and structural analyses* (Vol. 383, pp. 237–258). Boulder, CO: Geological Society of America.

Schmandt, B., & Humphreys, E. (2011). Seismically imaged relict slab from the 55 Ma Siletzia accretion to the northwest United States. *Geology*, *39*, 175–178. https://doi.org/10.1130/G31558.1

Scholl, D., Vallier, T., & Stevenson, A. (1986). Terrane accretion, production, and continental growth: A perspective based on the origin and tectonic fate of the Aleutian–Bering Sea region. *Geology*, *14*, 43–47.

Seabold, S., & Perktold, J. (2010). Statsmodels: Econometric and statistical modeling with Python. In *Proceedings of the 9th Python in Science Conference* (Vol. 57, p. 61). Scipy, Austin, Texas.

Seton, M., Flament, N., Whittaker, J., Müller, R., Gurnis, M., & Bower, D. (2015). Ridge subduction sparked reorganisation of the plate-mantle system 60–50 million years ago. *Geophysical Research Letters*, *42*, 1732–1740. https://doi.org/10.1002/2015GL063057

Seton, M., Müller, R., Zahirovic, S., Gaina, C., Torsvik, T., Shephard, G., et al. (2012). Global continental and ocean basin reconstructions since 200 Ma. *Earth-Science Reviews*, *113*(3-4), 212–270. https://doi.org/10.1016/j.earscirev.2012.03.002

Sibuet, J., Letouzey, J., Barbier, F., Charvet, J., Foucher, J., Hilde, T., et al. (1987). Back arc extension in the Okinawa Trough. *Journal of Geophysical Research*, *92*, 14,041–14,063.

Simmons, N.-A., Myers, S.-C., Johannesson, G., & Matzel, E. (2012). LLNL-G3Dv3: Global P wave tomography model for improved regional and teleseismic travel time prediction. *Journal of Geophysical Research*, *117*, B10302. https://doi.org/10.1029/2012JB009525

Spandler, C., Rubatto, D., & Hermann, J. (2005). Late Cretaceous-Tertiary tectonics of the southwest Pacific: Insights from U-Pb sensitive, high-resolution ion microprobe (SHRIMP) dating of eclogite facies rocks from New Caledonia. *Tectonics*, *24*, TC3003. https://doi.org/10.1029/2004TC001709

Stevenson, D., & Turner, J. (1977). Angle of subduction. *Nature*, *270*(5635), 334.

Sutherland, R., Barnes, P., & Uruski, C. (2006). Miocene-recent deformation, surface elevation, and volcanic intrusion of the overriding plate during subduction initiation, offshore southern Fiordland, Puysegur margin, southwest New Zealand. *New Zealand Journal of Geology and Geophysics*, *49*(1), 131–149. https://doi.org/10.1080/00288306.2006.9515154

Sutherland, R., Dickens, G., Blum, P., Agnini, C., Alegret, L., Asatryan, G., et al. (2020). Continental scale of geographic change across Zealandia during subduction zone initiation. *Geology*, *48*. https://doi.org/10.1130/G47008.1

Sutherland, R., Dickens, P., Blum, P., Agnini, C., Alegret, L., Asatryan, G., et al. (2019). Tasman frontier subduction initiation and paleogene climate. In *Proceedings of the International Ocean Discovery Program, Expedition 371* (pp. 1–307). College Station, TX. https://doi.org/10.14379/iodp.proc.371.101.2019

Taira, A., Ohara, Y., Wallis, S., Ishiwatari, A., & Iryu, Y. (2016). Geological evolution of Japan: An overview. In T. Moreno, T. Kojima, & W. Gibbons (Eds.), *Geology of Japan* (pp. 1–24). London: Geol. Soc.

Taylor, B. (1979). Bismarck Sea: Evolution of a back-arc basin. *Geology*, *7*, 171–174.

Tovish, A., & Schubert, G. (1978). Island arc curvature, velocity of convergence and angle of subduction. *Geophysical Research Letters*, *5*(5), 329–332.

Turcotte, D., & Schubert, G. (1982). Geodynamics: Application of continuum physics to geological problems. NY: Wiley.

Uyeda, S., & Kanamori, H. (1979). Back-arc opening and the mode of subduction. *Journal of Geophysical Research*, *84*(B3), 1049–1061.

van Hunen, J., van den Berg, A., & Vlaar, N. (2000). A thermo-mechanical model of horizontal subduction below an overriding plate. *Earth and Planetary Science Letters*, *182*(2), 157–169.

van Hunen, J., van den Berg, A., & Vlaar, N. (2004). Various mechanisms to induce shallow flat subduction: A numerical parameter study. *Physics of the Earth and Planetary Interiors*, *146*, 179–194.

Watson, B., & Fujita, K. (1985). Tectonic evolution of Kamchatka and the Sea of Okhotsk and implications for the Pacific Basin. In *Tectonostratigrahic terranes of the circum-Pacific region* (pp. 333–348). Houston TX: CircumPacific Council for Energy and Mineral Resources.

Wells, R., Bukry, D., Friedman, R., Pyle, D., Duncan, R., Haeussler, P., & Wooden, J. (2014). Geologic history of Siletzia, a large igneous province in the Oregon and Washington Coast Range: Correlation to the geomagnetic polarity time scale and implications for a long-lived Yellowstone hotspot. *Geosphere*, *10*, 692–719. https://doi.org/10.1130/GES01018.1

Wells, R., Engebretson, D., Snavely, P., & Coe, R. (1984). Cenozoic plate motions and the volcano-tectonic evolution of western Oregon and Washington. *Tectonics*, *3*, 275–294. https://doi.org/10.1029/TC003i002p00275

Wu, J., & Wu, J. (2019). Izanagi-Pacific ridge subduction revealed by a 56 to 46 Ma magmatic gap along the northeast Asian margin. *Geology*, *47*(10), 953–957. https://doi.org/10.1130/G46778.1

Yang, T., Moresi, L., Gurnis, M., Liu, S., Sandiford, D., Williams, S., & Capitanio, F.-A. (2019). Contrasted East Asia and South America tectonics driven by deep mantle flow. *Earth and Planetary Science Letters*, *517*, 106–116.

Yumul, G., Dimalanta, C., Maglambayan, V., & Marquez, E. (2008). Tectonic setting of a composite terrane: A review of the Philippine island arc system. *Geosciences Journal*, *12*, 7–17. https://doi.org/10.1007/s12303-008-0002-0

Yumul, G., Dimalanta, C., Tamayo, R., & Maury, R. (2003). Collision, subduction and accretion events in the Philippines: A synthesis. *Island Arc*, *12*(2), 77–91.

Zahirovic, S., Flament, N., Müller, R., Seton, M., & Gurnis, M. (2016). Large fluctuations of shallow seas in low-lying Southeast Asia driven by mantle flow. *Geochemistry, Geophysics, Geosystems*, *17*, 3589–3607. https://doi.org/10.1002/2016GC006434

Zhou, Q., Liu, L., & Hu, J. (2018). Western US volcanism due to intruding oceanic mantle driven by ancient Farallon slabs. *Nature Geoscience*, *11*(1), 70.